Acad Year
(2016/2017)
PROJECT NO.
A016

DESIGN AND MANUFACTURING OF A VTOL UAV BY 3D PRINTING

DESIGN AND MANUFACTURING OF A VTOL UAV BY 3D PRINTING

Tran Anh Thong

SCHOOL OF MECHANICAL AND AEROSPACE ENGINEERING
NANYANG TECHNOLOGICAL UNIVERSITY

Year (2016/2017)

STRENGTHENING AND DESIGN OPTIMIZATION FOR FUSED DEPOSITION MODELING PARTS FOR UAV APPLICATIONS

SUBMITTED

BY

TRAN ANH THONG

SCHOOL OF MECHANICAL AND AEROSPACE ENGINEERING

A final year project report

presented to

Nanyang Technological University

in partial fulfilment of

the requirements for the

Degree of Bachelor of Engineering (Mechanical Engineering)

Nanyang Technological University

Year (2016/2017)

TABLE OF CONTENTS

ACRONYMS AND ABBREVIATIONS

ABS	Acrylonitrile butadiene styrene
ASTM	American Society for Testing and Materials
CAD	Computer aided design
CAM	Computer aided manufacturing
CFRP	Carbon fiber reinforced polymers
CNC	Computer numerical control
EBM	Electron beam melting
FDM	Fused deposition modeling
LENS	Laser engineered net shaping
LOM	Laminated object manufacturing
PC	Polycarbonate
PLA	Polylactide
PPSF	Polyphenyl sulfone
SLS	Selective laser sintering
STL	Tessellation Language
UAV	Unmanned aerial vehicle

ABSTRACT

In this project, 3D printed parts are strengthened and optimized to study the feasibility of FDM technology in producing parts for unmanned aerial vehicles (UAVs). Two methods of reinforcing were studied: CFRP reinforcement and fill compositing. For CFRP reinforcement, the primary testing method was three-point bending. The samples were reinforced by applying unidirectional CFRP prepregs on the top and bottom surfaces with adhesive. The results showed that the method was capable of significantly increase the load and stiffness of the part with consistency. For fill compositing method, L-shaped samples were used in a bending test setup. Initial results showed improvements in both load and stiffness. The methods to further alleviate possible errors during experiments and sample preparation can be achieved by further investigating the reinforcement technique on the suitability of application to the structure. Furthermore, topology optimization was done to realize the optimal designs for the L-shaped sample. For future studies, this can be implemented with reinforcing methods for optimal performance in strength to weight of the part.

ACKNOWLEDGEMENT

I would like to first and foremost to thank Professor Erdal Kayacan, my final year project supervisor, for providing me with the opportunity to work on this project. I am very grateful to have the chance to work under your supervision and guidance.

To Ravindrababu Suraj, my mentor, without whom this project would not have been possible. He has supported me throughout the whole project and gave me valuable knowledge and suggestion when I needed.

Also to Govdeli Yunus, Wong Zhou Wei, and other members of the Flight Mechanics and Control lab, for their help during the project. It is a pleasure to be able to work with you.

Lastly, I would like to thank Mr. Lim Yong Seng, Mr. Sa'don Bin Ahmad and Ms. Chia Hwee Lang for allowing access and giving instruction to use all the necessary materials and equipment for the project. I am also extremely thankful to administrative staffs and students of MAE for their aiding to this project.

List of Figures

List of Tables

1. INTRODUCTION

1.1. Background

Unmanned aerial vehicles (UAVs) has been an ongoing subject of studies and researches. For this purpose, certain requirements in term of structure need to be met. As parts for UAVs often are complicated, a manufacturing method that can be used with a wide range of intricate designs like 3D printing is preferable. However, for the parts to operate reliably in flying conditions, reinforcement and optimization need to be done to improve their strength as well as reduce material. This project aimed to study such strengthening methods. Strengthening techniques were studied and applied to improve the quality of 3D printed material. Topology optimization was carried out to enhance the designs of parts. This served to further customize the part for particular loading conditions and reduce its material volume. The end results should be parts with better mechanical properties such as strength stiffness, and with optimal design in term of structure and weight that they perform under loads as well as adverse phenomena such as aeroelastic fluttering.

1.2 Objectives and scope

The project presented in this report was taken on to study reinforcement methods that can be utilized to strengthen 3D printed parts for UAVs. The two methods studied were CFRP reinforcement and fill compositing. Topology optimization was also studied to be applied to the design phase in future studies. The project aims to:

- Fabricate and test 3D printed samples strengthened by different methods.
- Draw conclusions on the performance of each method (comparing strength to weight ratio, modes of failure, feasibility).
- Optimizing structural designs for more efficient parts
- Make recommendations to improve each method.
- Implement the studied methods on designed parts to observe improvement in performance.

2. LITERATURE REVIEW

2.1. 3D printing technology

3D printing, or additive manufacturing, is a process of forming a 3D object by adding material layer by layer. The general process begins with creating a CAD file of the object, which is then converted to a standardized file format, such as the Standard Tessellation Language (STL). Next, the file is transferred to the machine or a software where its position, orientation, and scaling are defined and the model is sliced into layers of uniform thickness. Tool paths are generated to form the profile of each layer. The final step is the building of the object layer by layer. The build process can be divided into two sub-processes: the printing and the joining of each layer, which are done simultaneously. [1-3]

3D printing is a combination of other technologies including computer aided design (CAD), computer aided manufacturing (CAM), and computer numerical control (CNC). There are numerous 3D printing techniques; some of them are stereolithography (SLA), fused deposition modeling (FDM), Polyjet, laminated object manufacturing (LOM), selective laser sintering (SLS), electron beam melting (EBM), laser engineered net shaping (LENS). [2, 3]

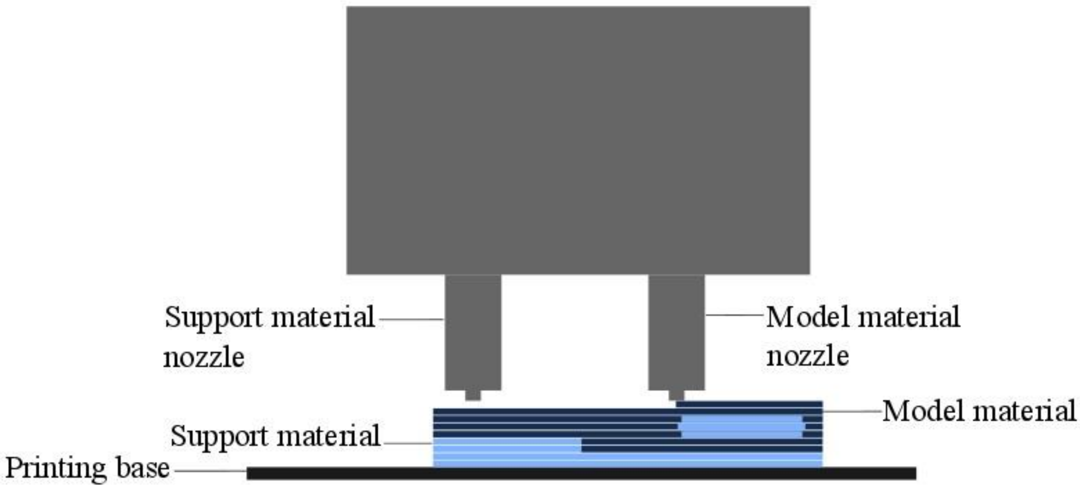

Figure 2-1 Fused Deposition Modeling.

Fused deposition modeling process involves injecting liquid thermoplastic through a nozzle or print head to form thin layers of material, which would build up into the part. A filament of the material is fed into the machine, where it would be heated to slightly higher than its melting point so that the material would solidify immediately after being injected to form the layer. Some of the thermoplastic materials that can be used with the process are polycarbonate (PC), polyphenyl sulfone (PPSF), polylactide (PLA), acrylonitrile butadiene styrene (ABS). An additional nozzle can be added to print the support material, which is cheaper and can easily be removed after printing. Despite being cost-effective, FDM has some disadvantages including long build time for complex geometry, the requirement of support structure, low resolution in z direction. Furthermore, delamination between the layers causes the strength of the part to be influenced by the printing direction.[2-8]

2.2. Carbon fiber reinforced polymers (CFRP) reinforcement

CFRP is a composite material consisting of two part. The first part is the fiber, which is made of carbon strands; the second part is the matrix, which can be an epoxy or resin. Carbon fiber is a material with a very high strength to weight ratio, good dimensional stability, high tensile strength (up to above 500 GPa), but also brittle. Carbon fiber filaments can be as thin as 7 to 10 microns. Multiple filaments of carbon fiber are combined to form a carbon fiber strand, which is woven into a fabric sheet of carbon. The fabric is then impregnated with epoxy or resin material to form CFRP.[9-12]

CFRP inherit some key characteristics of carbon fiber such as high strength to weight, high fatigue strength, high elasticity modulus, and corrosion resistance. Thus, it is widely used in demanding applications such as aerospace, general industry, automobiles, military structures, sports equipment. [11, 13]

CFRP is an anisotropic material since its strength depends mostly on that of the fiber. Hence, it displays high strength in the fiber direction while has a much lower strength in the transverse direction.

CFRP as a strengthening add-on material was primarily used for reinforced concrete structure such as columns and beams of bridges or building. The CFRP can be wrapped around or applied to the surfaces of the structures, where high stress is anticipated. This type of reinforcement has two main modes of failure: rupture and debonding. In the case of rupture, the carbon fiber would reach its ultimate stress and strain value. On the other hand, debonding happens before the CFRP reaches its full strength. The reinforcement instead comes apart from the reinforced substrate because of interfacial failure originating in between the layers of CFRP. It is more desirable to have the rupture mode of failure as it means the strength of the CFRP is fully utilized.[11, 14]

2.3. Fill compositing

FDM parts can be strengthened using fill compositing technique. Using this strengthening method, strength and stiffness can be improved. The test samples were printed from ABS plastic. The technique was tested in a study with numerous resin and epoxy, such as Smooth-cast 305 resin, IE-3076 urethane, and West Marine 105-206. In additional, glass fiber and wollastonite was added to the resin to test the possibility of further strengthening the parts.

The fill composite technique uses hollow voids and channels in the components as molds for the strengthening material. There are three methods to create the hollow voids within the part. The first one is to print with sparse infill, which does not require any changes to the design of the parts. The second method is to make the part completely hollow. The outer wall of the parts would act as the mold to cast the stronger composite material. This method's limitation is the capability of the printer to create the voids without support material. The third method is to design channels in desired regions that need strengthening based on the expected loading. This method is efficient as the parts have the highest strength to weight ratio since there is only resin in appropriate regions. The strengthening material is injected using a syringe. The injection sites are chosen so that casting material will not leak to infill holes. It is preferred to have vent holes as there may be air trapped in the injection process. The technique is similar to investment casting as the part is used as a mold for the stronger strengthening material.

3D printed parts can be enhanced using the fill composite technique, even in the most preferable print orientation. The epoxy filled shell samples display higher strength to weight ratio compared to solid ABS printed in any orientation. The epoxy filled channel samples have the highest stiffness to weight ratio with all epoxy infills.

Overall yield strength and stiffness of the hollow printed filled with epoxy were higher than that of solid ABS. For epoxy filled channels samples, strength and stiffness to weight ratio also increase. Strength limitation of the worst print orientation can be overcome using the technique. The limitation of the technique is that the parts need to be printed with non-porous internal voids, which can be mitigated by adjusting printing settings to prevent cavities from forming.[15]

2.4. Topology optimization

Topology optimization is the process of distributing a given amount of material in a prescribed space to achieve an optimal performance. The technique can be used in many settings, to achieve design goals for mechanical structures, electromagnetic, or acoustic devices.[16-19] Stiffness designs is a traditional topology optimization problem. The process is aided with finite element method. Base on the design constrain and loading, each element can be added or eliminated through each iteration until convergence is reached.

Topology optimization techniques include evolution based algorithms, solid isotropic microstructure with penalization, evolutionary structural optimization methods, soft-kill option, and level-set methods. The first four methods involve changing the density of elements or removing them from the structure while the level-set methods aim to optimize the auxiliary continuous function that represents the structure volume. [20]

The optimized structures, however, may be impossible to be manufactured by traditional methods due to their complex geometries. This problem can be solved by utilizing additive manufacturing, which allows a high freedom in designs. [21]

3. MATERIALS

3.1. 3D printing material

For this project, the model material used for 3D printing is ABS. Since the printing was done by the Dimension Elite, ABSplus-P430 filament supplied by Stratasys was used for all the samples. ABSplus-P430 is a production grade thermoplastic which comes in filament form contained in cartridges.[22] Some of its properties as provided by Stratasys are listed below:

Table 3-1 ABSplus-P430 Properties.

Ultimate Tensile Strength	33 MPa
Yield Strength	31 MPa
Tensile Modulus	2200 MPa
Tensile elongation at break	6%
Tensile elongation at yield	2%
Flexural strength	58 MPa
Flexural modulus	2100 MPa
Flexural strain at break	2%

Support material for printing is P400SR produced by Stratasys. P400SR also comes in filament form in cartridges. P400SR is a soluble support material which can be removed in a warm solution of water and sodium hydroxide. The heated solution would melt away P400SR, leaving the model material unharmed.

Figure 3-1 Cartridges for ABSplus-P430 model material and P400SR support material of the Dimension Elite 3D printing machine.

3.2. CFRP

The CFRP used in this project is AX-6200-C from Axiom Materials. This is a toughened epoxy unidirectional carbon laminating prepreg.

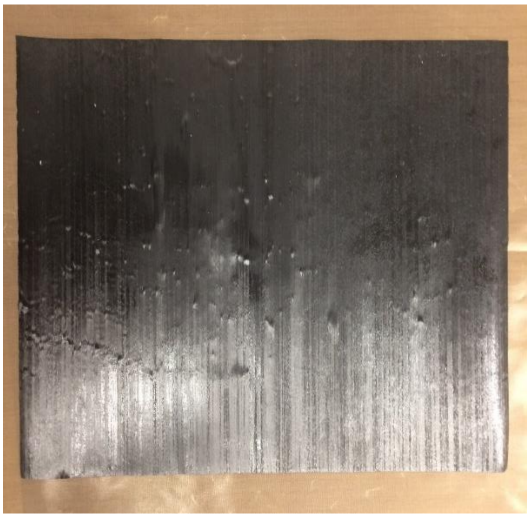

Figure 3-2 Uncured AX-6200-C CFRP sheet.

The CFRP is stored at a temperature below 4°C and cured at 120°C for 2 hours.[23] Some of the key properties as stated by the Axiom Materials are listed below:

Table 3-2 CFRP properties.

Resin content by weight	32-38%
Fiber tensile strength	4.9 GPa
Fiber tensile modulus	230 GPa
Fiber elongation	2.1%
Fiber density	1.79g/cm^3

3.3. Adhesives

In this project, three types of adhesive were used for the experiments: Redux 335K, Araldite epoxy, and Alteco Superglue 110. The three adhesives chosen were different in term of type, curing process, cost, and availability. Redux 335K is a film adhesive; Araldite is a two-part epoxy; Alteco Superglue 110 is a cyanoacrylate adhesive. Curing of Redux 335K requires heat curing while Araldite and Alteco adhesive cures at room temperature in 14 hours and one minute respectively. In term of availability, Redux 335K is a specialized adhesive that comes in bulk quantity; Araldite and Alteco adhesive are commercial adhesives available in small quantity. These factors decide the time and cost requirements, the complexity of the reinforcing method, and consequently, the feasibility of it.

Redux-335K is a blue film adhesive with a weight per unit area of 300 g/m^2. It has reliable performance with 120^{o}C – curing fiber reinforced composites. The adhesive is packed in between a layer of paper and a polythene backing sheet, which would be removed before applying to the bonding surface. At room temperature, the adhesive has lap shear strength of 39-43 MPa (Lap shear strength is the strength of the adhesive when tested on a single lap-joint sample).[24]

Araldite epoxy is a multipurpose two-part epoxy with room temperature curing. The epoxy is created by mixing the resin and hardener at 1:1 ratio by volume. A curing time of at least 14 hours is recommended for the epoxy to cure to full strength at room temperature. The lab strength for Araldite epoxy varies with the substrate material (5.5MPa for ABS, 16.5 MPa for wood, 19 MPa for aluminum).[25]

Figure 3-3 Araldite two-part epoxy.

Alteco Superglue 110 is a multipurpose commercial cyanoacrylate adhesive. It cures at room temperature in under 1 minute. The minimum shear strength of the adhesive is 9.8 MPa.[26]

Figure 3-4 Alteco Superglue 110 Cyanoacrylate adhesive.

3.4. Epoxy Resin

For fill compositing technique, the samples were reinforced using Epolam 5051 epoxy resin from Axon Technologies. The mixing ratio by weight of resin and hardener is 100:30. This is a low viscosity epoxy resin that can be cured at room conditions. A post cure process at 60^oC for 120 minutes is recommended to enhance the material properties.[27] The epoxy resin properties are as followed:

Table 3-3 Epolam 5051 properties.

Flexural modulus	3000 MPa
Maximum flexural strength	105 MPa
Tensile strength	80 MPa
Elongation at break	6%
Mixing viscosity at 25^oC	1.1 mPa.s

4. SAMPLE PREPARATION

4.1. Sample designs

The CADs for samples used in the experiments are created using Solidworks software. Several different designs were created for each type of test and reinforcement methods.

For CFRP reinforcement, samples with rectangular cross section were created accordingly with the ASTM D790 standard for test methods for flexural properties of plastics. The dimension is as followed: 150×12.7×3.2mm. These samples would later be used for 3-point bending tests to determine the flexural stiffness of the reinforced material.

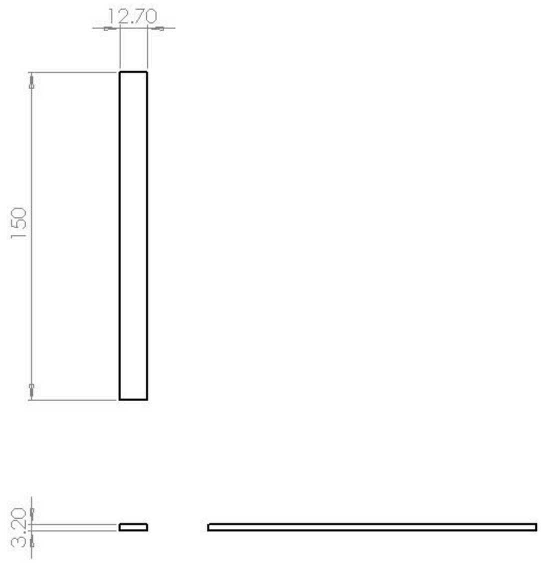

Figure 4-1 Three-view drawing of three-point bending sample.

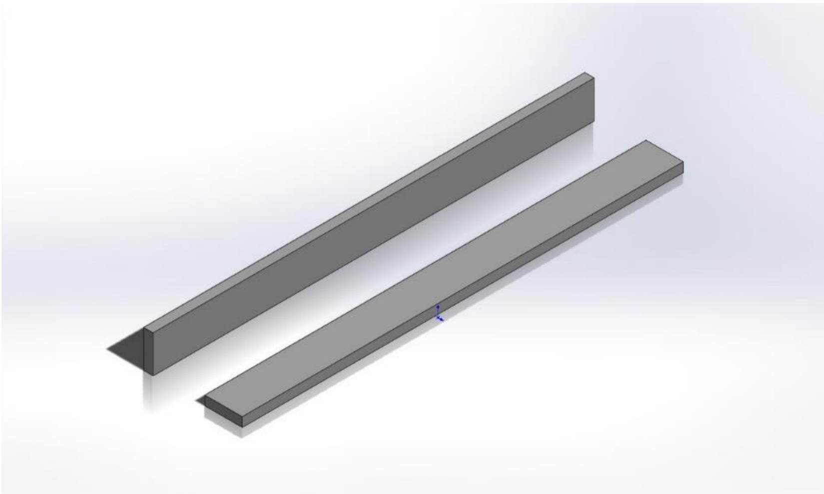

Figure 4-2 Two orientations for printing of three-point bending sample (edge-up orientation on the left, face-up orientation on the right).

For fill compositing method, the designs must include voids to be filled with reinforcing resin. At first, gaps and channels were added to the rectangular cross section with the same dimension as above. However, because of constraints in term of printing accuracy, such designs were not feasible.

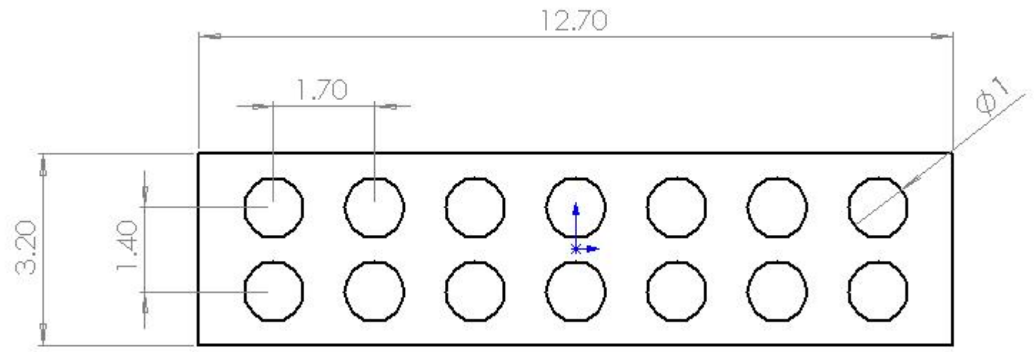

Figure 4-3 Cross-section of ‘channel’ designs for fill compositing sample.

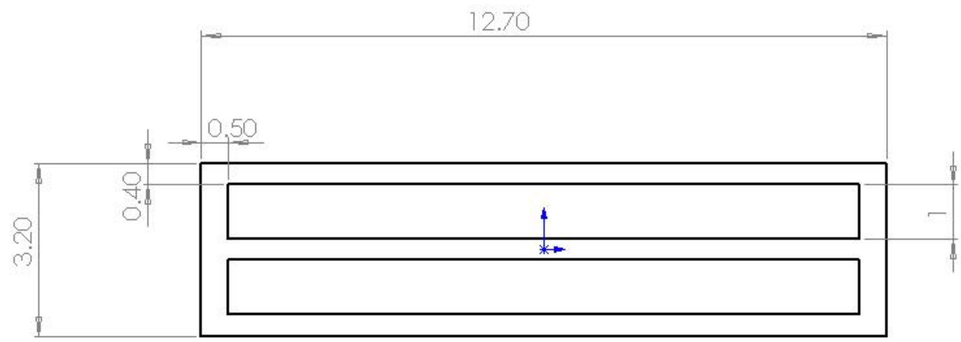

Figure 4-4 Cross-section of ‘gap’ designs for fill compositing sample.

Thus, another design was created to test the fill compositing method. L-shaped samples with an I-shaped cross section with channels were used for a different bending test method. This design was also used to test CFRP reinforcements to compare the two methods.

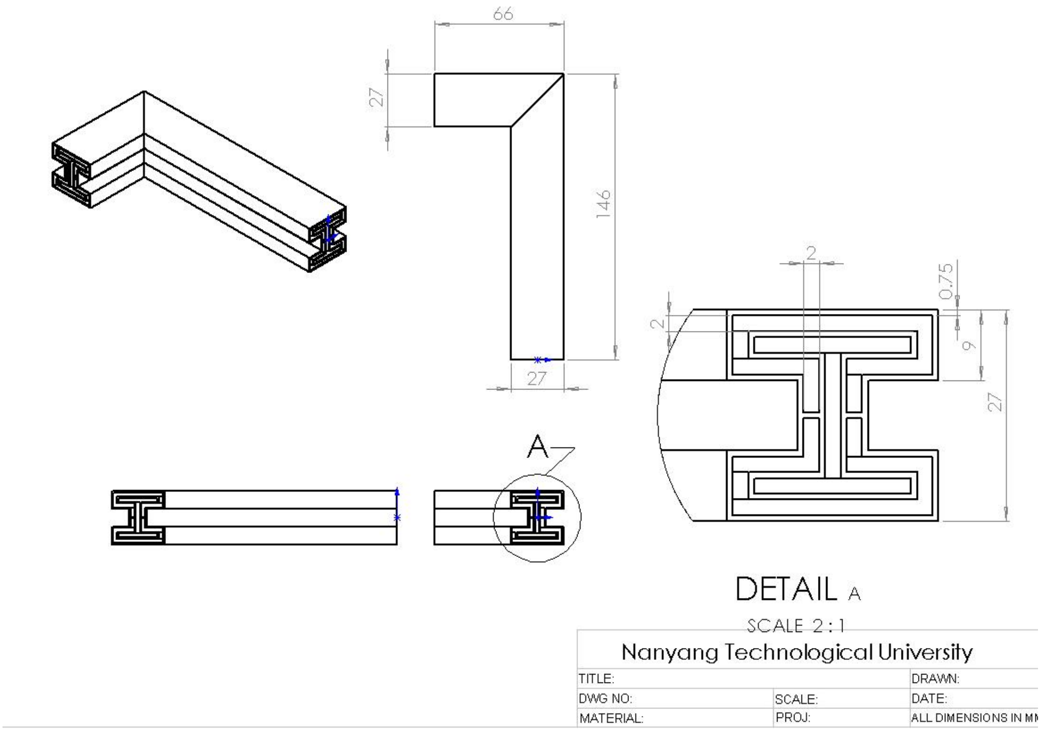

Figure 4-5 CAD design of L-shaped sample for fill compositing.

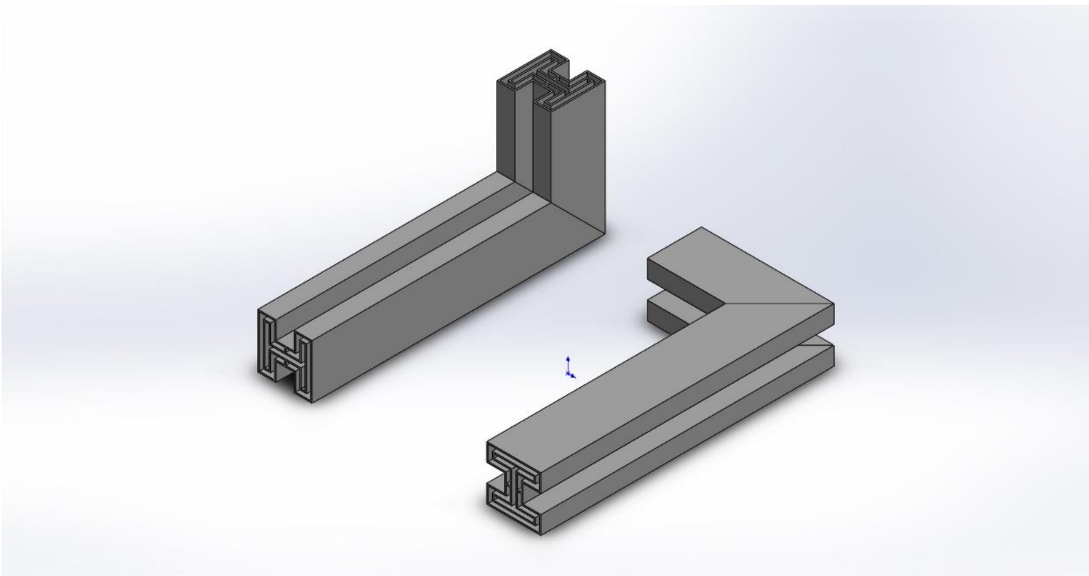

Fig 4-6 Two orientations for printing of L-shaped sample for fill compositing (edge-up orientation on the left, face-up orientation on the right).

Motor arm designs were also created to test with both methods. A solid design was use for the CFRP reinforcing method

4.2. Fabrication of 3D printed samples

Samples were printed with Stratasys Dimension Elite 3D printer. The machine has a layer thickness of 0.178mm (0.007 inch) and accuracy of ±0.200mm. The procedure is as followed:

1. An STL file of the sample design is created with Solidworks.
2. The file would then be inputted in the CatalystEX software of the printing machine. The setting of the software would be adjusted to solid model and sparse support.
3. The software would then be used to orient the samples to proper positions and add support structure to the sample. Tool path for each specific part would be generated and saved as CMB files, which can be multiplied to form a pack for printing.
4. The pack was added to the queue, with estimated time and material.
5. Remove any printed parts or uses printing plate.
6. Add the new printing plate in the machine.
7. Remove unwanted cartridges (if any) by pressing unload in the control panel of the machine.
8. Load the appropriate cartridges for model and support material in the designated slot and press load on the control panel.
9. Purge the printing nozzle to remove remaining materials and to make sure that the new material was properly loaded.
10. Calibrate the machine to make sure the plate was leveled properly.
11. Begin printing the queue as inputted in the software.
12. Remove the printing plate with the complete printed part.
13. Detach the printed parts and remove parts of the support manually. Deposit the printed parts in the Waterworks bath to dissolve any remained support structure.

For this project, ABS was used for model and P400SR for support. Images of the 3D printing equipment and software can be found in Appendix A

4.3. Prepreg preparation

AX-6200-C prepreg produced by Axiom material was used for this project, with the exception of the experiment on the motor arm. The prepregs are cut to fit on the surface of the reinforced parts. The direction of the fiber oriented to align with the length of the rectangular samples and motor arm sample, the long leg of the L-shape samples and the length of the motor arm.

Figure 4-7 Strips of CFRP cut for three-point bending samples

After cutting, the prepregs are laid down on coated fiberglass paper to prevent sticking. Most of the prepregs are cured while being laid on a flat surface. If they would later be applied on a curved surface, they would be co-cure on the same surface to create the necessary curvature. Weights are applied on top to ensure that the shapes of the prepregs are as desired. The curing process is 2 hours long at 120^{o}C.

Figure 4-8 Binder oven for curing processes.

4.4. Applying prepregs on printed parts

Prepregs were applied to the printed parts using adhesives. Initial tests to co-cure the adhesive and prepregs for the Redux 335K adhesive produced undesirable results as the expansion rate different between the materials would cause deformation and prestress the samples.

For the case of the Redux 335K adhesive, the adhesive was cured in the oven at 120^{o}C for 2 hours after applying the cured prepreg to the surface of the samples. For two-part Araldite epoxy, the epoxy resin is mixed and apply between the CFRP prepregs and ABS samples and leave for one day to set. For Cyanoacrylate Alteco adhesive, the set time was 1 minutes and the samples would be ready to be tested in 1 hour after applying.

In all cases, weights were used to apply pressure and ensure proper contact between the adhesive and materials and prevent any prestress.

4.5. Applying prepregs on the motor arms

The CRFP used for the motor arm was bidirectional woven (0^{o}/90^{o}) prepreg. Cyanoacrylate adhesive was used to apply the CFRP reinforcement to the surfaces of the motor arm. As one of the two faces chosen to be applied with the CFRP is a curved surface, the respective CFRP was cured while being placed on the part itself to make sure that the cured CFRP could adhere properly to the part.

4.6. Fill compositing sample curing process

Epolam 5051 resin was used to make the fill compositing samples. The resin and hardener were mixed thoroughly at 100:30 ratio. The sample cured at room temperature for a day before being post-cured at 60^{o}C for 2 hours in the oven to further enhance its properties.

5. EXPERIMENT METHODS

5.1. Three-point bending method

Three-point bending tests were carried out for rectangular cross section samples reinforced with CFRP. The test was done following the guidelines of ASTM D790 with the Instron 5569 materials testing machine with a load cell of ±50kN.

Figure 5-1 Instron 5569 materials testing machine.

The procedure was as followed:

1. Measure the depth (or thickness) of each sample at the center of the support span. The samples were measured to at least the nearest 0.02mm. The weight of the sample would also be measured to 0.01g.
2. The span for all three-point bending tests done in this project was determined to be 50mm. The flexural fixture was adjusted to this setting.
3. Calculate the rate of descending motion for the loading nose [28] as follow:

$$R = ZL^2/6d$$

   With:
   R = Rate of loading nose motion, mm/min,
   Z = Rate of straining of outer fiber, mm/mm/min. In this case, Z was 0.01,
   L = Length of support span, mm,
   d = Depth or thickness of sample, mm.
4. The fixture is adjusted so that the loading nose axis is parallel to those of the supports and the loading nose is midway between the supports.
5. Place the specimen on the support so that it centers the fixture and the length of the specimen is perpendicular to the axes of the loading nose and the

supports. Lower the loading nose until it is just above contact with the specimen.

6. Input the parameters to the software, including the span, width, thickness and rate of motion as calculated. Reset the loading and strain gauge to zero.
7. Begin testing. The Bluehill software would record all load and deflection data during the test.
8. Stop the test when the sample reaches maximum strain or when breaks occur.
9. Parameterized flexural stiffness is calculated for the Hookean region as follow:

$$K_t = F/xd^3$$

With:

K_t = Parameterized Flexural Stiffness, N/mm^4,

F = Load, N,

x = Displacement or extension, mm,

d = Depth of the sample, mm.

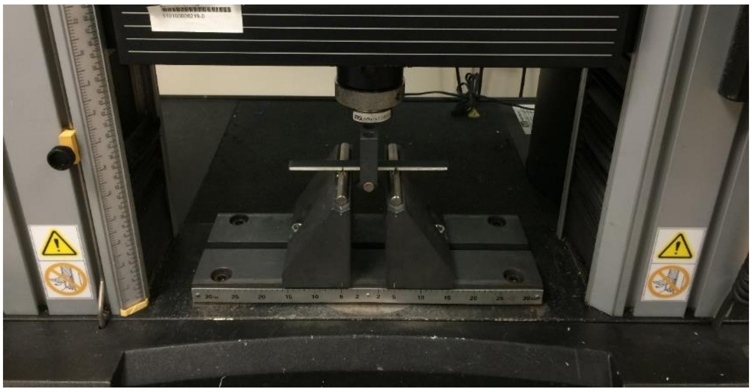

Figure5-2 Three-point bending experimental setup.

The data that could be collected and calculated from the tests included the load-extension curve, the maximum load, load and extension at failure, failure mode, flexural stiffness, and parameterized flexural stiffness with regard to thickness.

5.2. Bending test of the L-shaped samples

The tests for bending the L-shaped samples also use the Instron 5569 with a ±50kN load cell. The procedure was as followed:

1. Measure the weight of the samples to 0.01g.

2. Set up the clamp and fix the loading nose to the testing machine. The outer edge of the clamp was placed 11.5cm from the center of the support base.
3. The rate of displacement for the loading nose was set to 5mm/min.
4. The clamp was fixed to the base and the loading nose is set at the horizontal position, parallel with the length of the support base.
5. The long end of the L-shaped sample was securely fixed between the surfaces of the clamp so that it is positioned lengthwise with respect to the support base.
6. Reset the strain and loading gauge of the machine to zero.
7. Start testing.
8. Stop the test when the sample reaches maximum strain or breaks occurs.
9. Calculate flexural stiffness coefficient:

$$k = F/x$$

   With:

   k = Flexural stiffness coefficient, N/mm,

   F = Load, N,

   x = Displacement or extension, mm.

The samples were subjected to both bending and torsion during testing due to the complex loading condition. The extension-loading curves were obtained along with the maximum load and extension at failure, failure mode. The flexural stiffness coefficient was calculated in the Hookean region for each sample.

Figure 5-3 Bending test setup.

6. RESULTS

6.1. There-point bending of rectangular cross-section samples

6.1.1 Bare ABS samples

The samples were tested in face-up and edge-up configuration with three samples each. The procedure was three-point bending as stated above. The following are measurements of the samples prior to the tests and the results of the tests. Individual Load – Extension curves of samples can be found in Appendix B.

Table 6-1 Bare ABS Three-point bending samples' measurements.

Sample	Configuration	Thickness (mm)	Weight (g)	Length (mm)
1	Face-up	3.34	5.99	150
2	Face-up	3.26	5.98	150
3	Face-up	3.30	5.99	150
4	Edge-up	3.14	5.92	150
5	Edge-up	3.14	5.92	150
6	Edge-up	3.14	5.92	150

Table 6-2 Bare ABS Three-point bending test results.

Sample	Max Load (N)	Extension at max load (mm)	Parameterized Flexural Stiffness (N/mm^4)
1	99.95	7.007	0.729
2	100.14	6.491	0.774
3	98.03	6.287	0.722
4	99.43	6.116	0.809
5	98.07	6.069	0.837
6	98.74	6.257	0.813

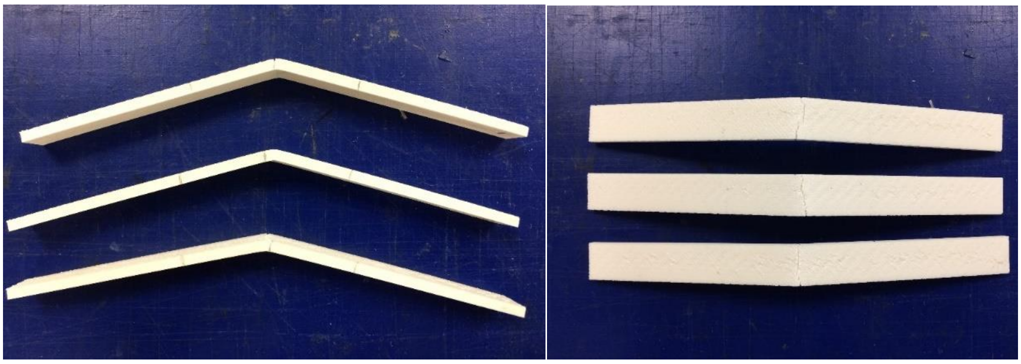

Figure 6-1 Post-test bare ABS samples.

All samples failed in similar manners at the point of contact with the loading nose. Fractures due to stress at the lower surface can be observed in each case. The loading curves obtained were that of typical plastic material under large bending deformation.

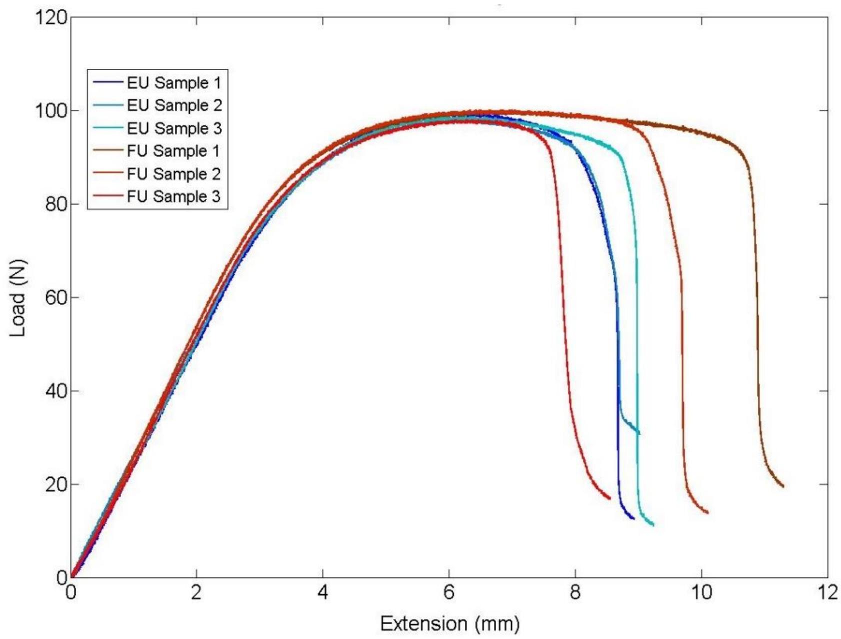

Figure 6-2 Loading curves of bar ABS three-point bending samples.

6.1.2. CFRP Reinforced samples with rectangular cross section

For tests of CFRP Reinforced samples, mode of failure of the samples are observe along with other parameters such as load, extension, flexural stiffness. As materials were added to reinforce the samples, increase in weight of each sample was also a factor to consider.

6.1.2.1. Redux 335K adhesive

Three samples were tested (two face-ups and one edge-up). The test was three-point bending. Individual Load – Extension curves of samples can be found in Appendix.

Table 6-3 Redux Three-point bending samples' measurements.

Sample	Configuration	Thickness (mm)	Weight (g)	Length (mm)	Percentage increase in weight
1	Face-up	3.95	6.813	127	34.3
2	Edge-up	3.72	8.4358	150	42.5
3	Face-up	3.94	8.8321	150	47.4

Table 6-4 Redux three-point bending test results

Sample	Max Load (N)	Extension at max load (mm)	Parameterized Flexural Stiffness (N/mm4)	Mode of failure
1	602.95	1.115	8.76	CFRP Rupture
2	276.39	0.619	9.1	Adhesive debonding
3	319.88	0.681	7.57	Adhesive debonding

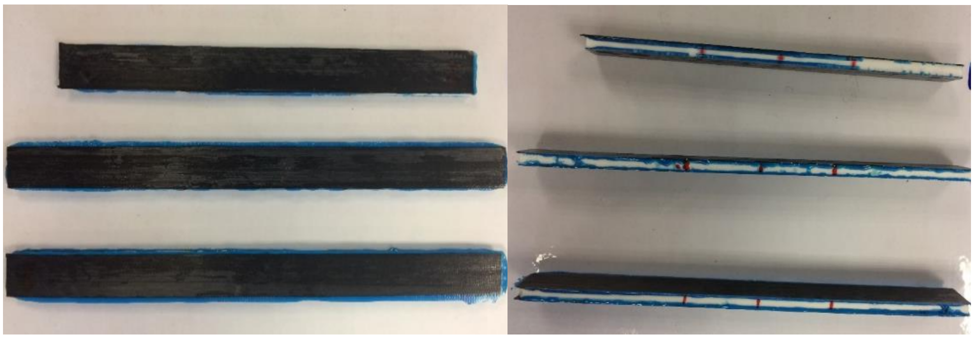

Figure 6-3 Redux CFRP reinforced samples.

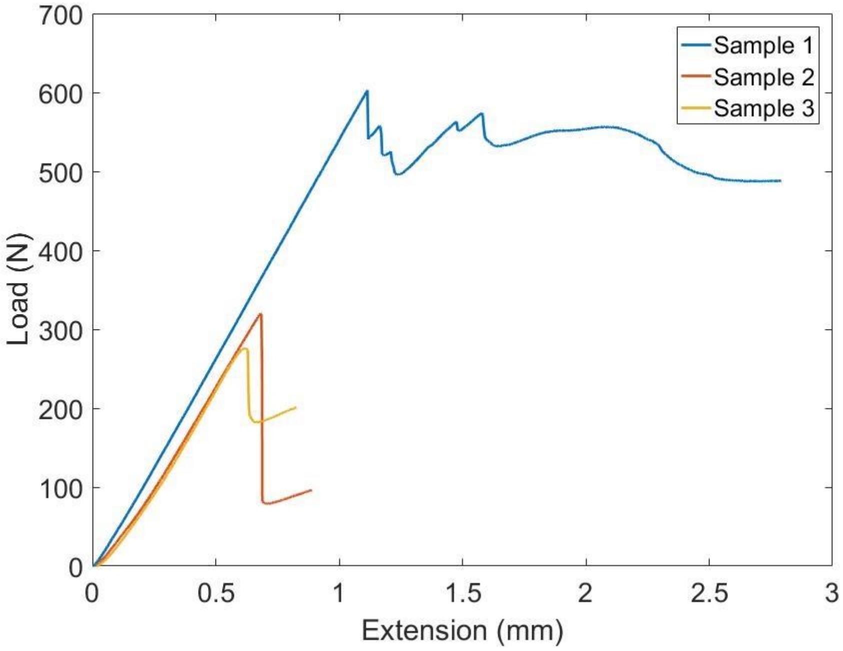

Figure 6-4 Loading curves of Redux samples.

None of the samples had signs of failure in the ABS material. However, sample 2 and 3 had a much different behavior compared to that of sample 1. As we can see from figure 6-4, the two samples that failed by debonding has significantly lower maximum load while having no progressive failure that sample 1 had. Sample 1 had fractures on the CFRP top ply due to the compression loading why the top ply debonded for samples 2 and 3.

6.1.2.2. Araldite Epoxy

Four sample was tested (two face-ups and two edge-up) with three-point bending method. The measurements and test results are below.

Table 6-5 Araldite three-point bending samples' measurements.

Sample	Configuration	Thickness (mm)	Weight (g)	Length (mm)	Percentage increase in weight
1	Face-up	3.9	7.942	150	32.6
2	Face-up	3.94	8.069	150	34.7
3	Edge-up	3.96	7.912	150	33.6
4	Edge-up	3.99	7.957	150	34.4

Table 6-6 Araldite three-point bending test results

Sample	Max Load (N)	Extension at max load (mm)	Parameterized Flexural Stiffness (N/mm^4)	Mode of failure
1	473.109	0.919	8.68	Adhesive debonding
2	419.885	0.821	8.41	Adhesive debonding
3	567.352	1.11	8.25	Adhesive debonding
4	583.285	1.31	7.77	Adhesive debonding

The samples reinforced with Araldite epoxy had comparable results. All samples failed by debonding between top ply of CFRP and ABS due to compression. There was no progressive failure during the loading in any of the samples. The CFRP plies were found to be undamaged in all the sample despite the debonding. The ABS material also had no visible sign of damage in any of the samples.

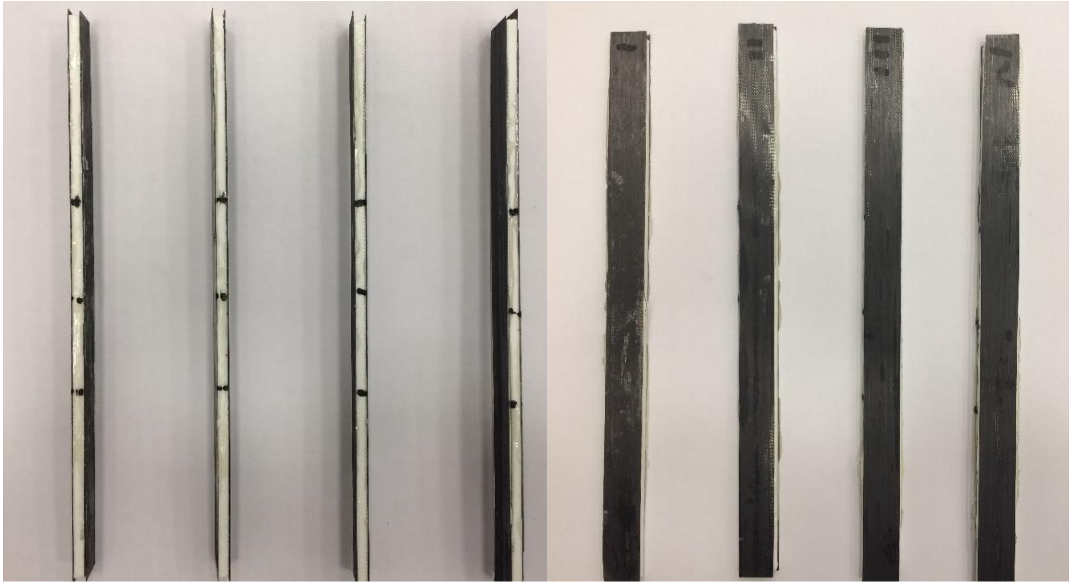

Figure 6-5 Araldite CFRP reinforced samples.

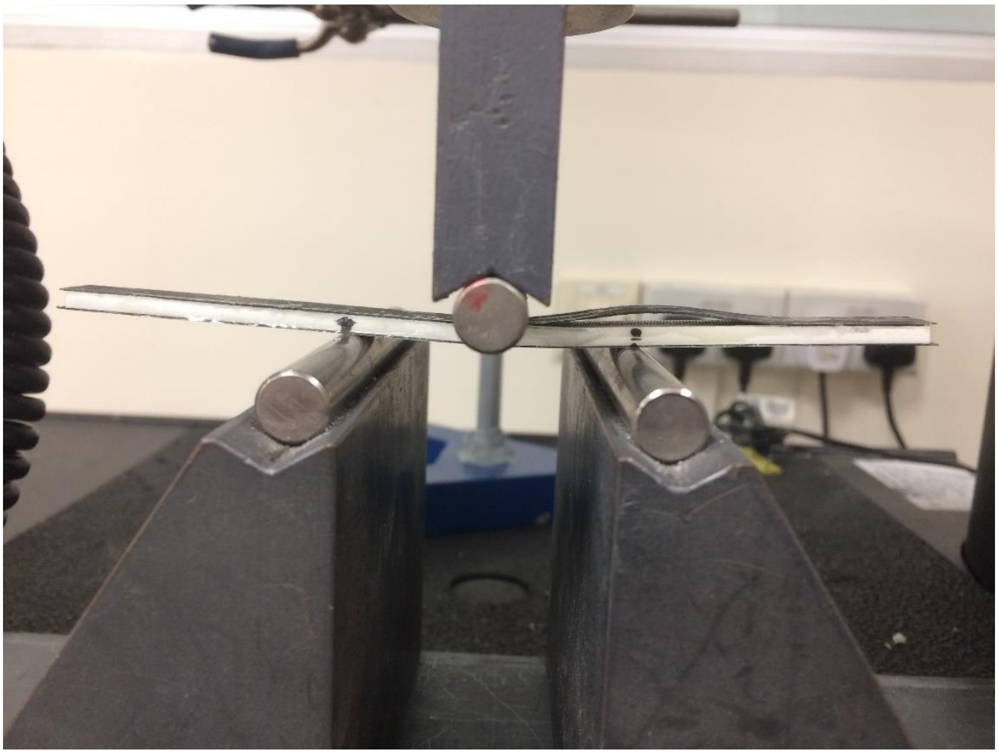

Figure 6-6 Debonding occurred during testing in one of the Araldite samples.

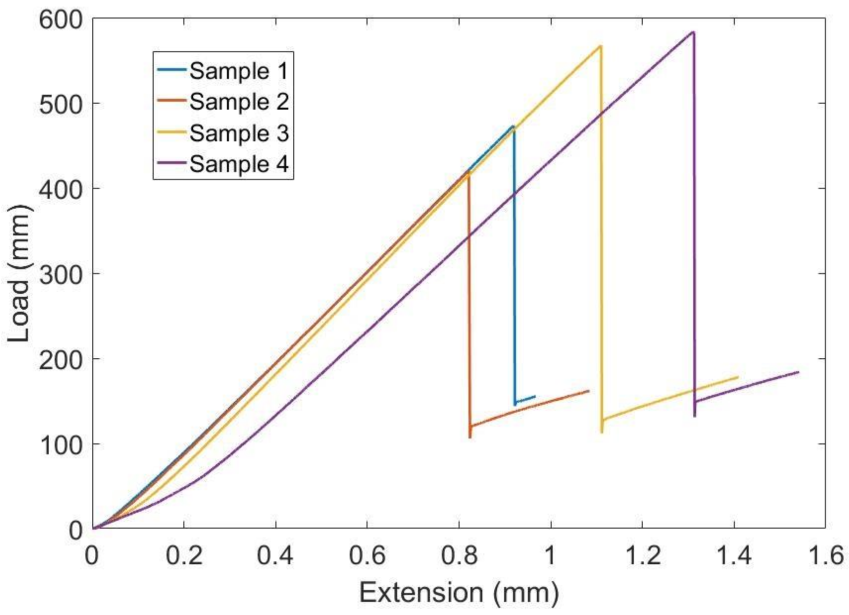

Figure 6-7 Loading curves of Araldite samples.

Individual Load – Extension curves of samples can be found in Appendix B.

6.1.2.3. Alteco Cyanoacrylate adhesive

Four face-up samples were tested with three-point bending method. The measurements and test results for the samples are shown below.

Table 6-7 Alteco three-point bending samples' measurements.

Sample	Configuration	Thickness (mm)	Weight (g)	Length (mm)	Percentage increase in weight
1	Face-up	4.04	8.072	150	34.8
2	Face-up	4.05	8.007	150	33.7
3	Face-up	3.96	7.966	150	33.0
4	Face-up	4.03	8.15	150	36.1

Table 6-8 Alteco three-point bending test results.

Sample	Max Load (N)	Extension at max load (mm)	Parameterized Flexural Stiffness (N/mm4)	Mode of failure
1	670.558	2.241	8.58	CFRP Rupture
2	666.322	2.154	8.7	CFRP Rupture
3	663.314	2.069	9.34	CFRP Rupture
4	685.713	3.33	8.01	CFRP Rupture

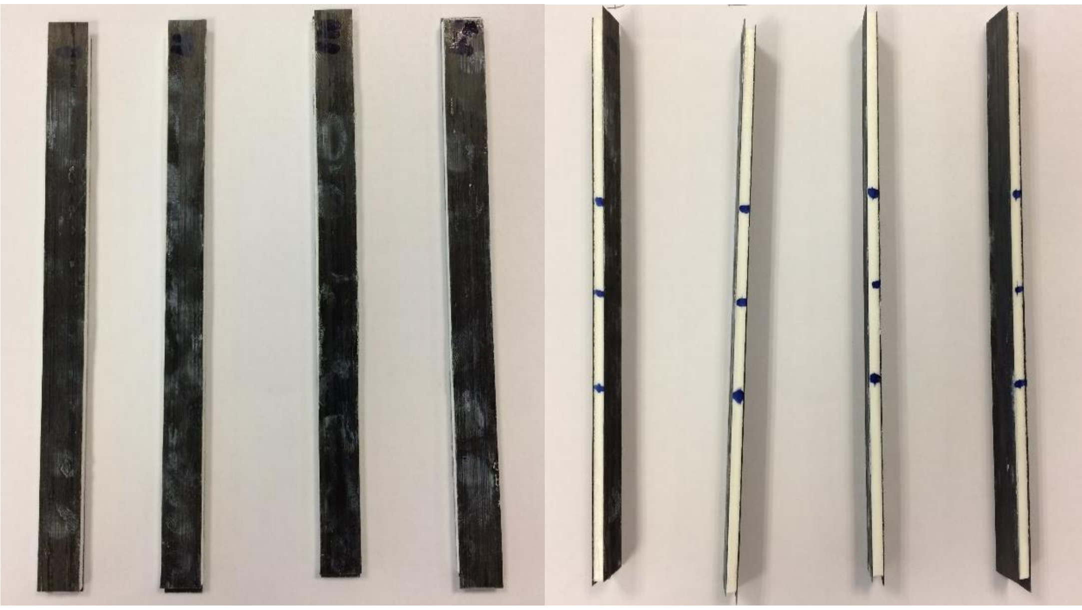

Figure 6-8 Alteco CFRP reinforced samples.

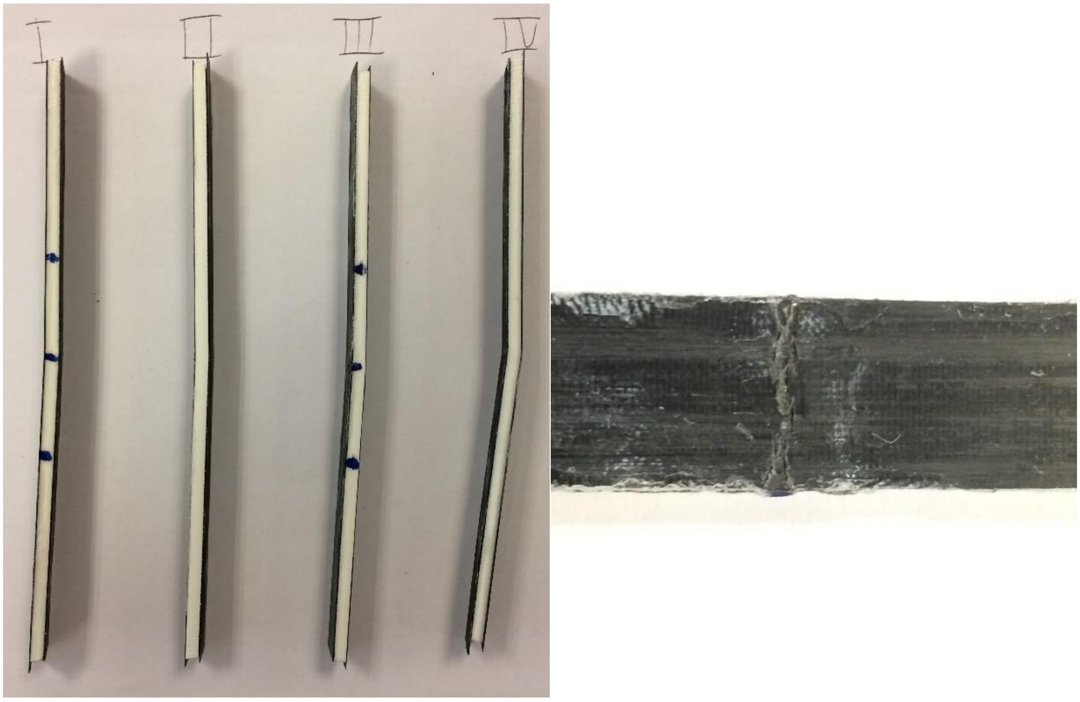

Figure 6-9 Post-test Alteco samples (left), and CFRP rupture on one of the samples (right).

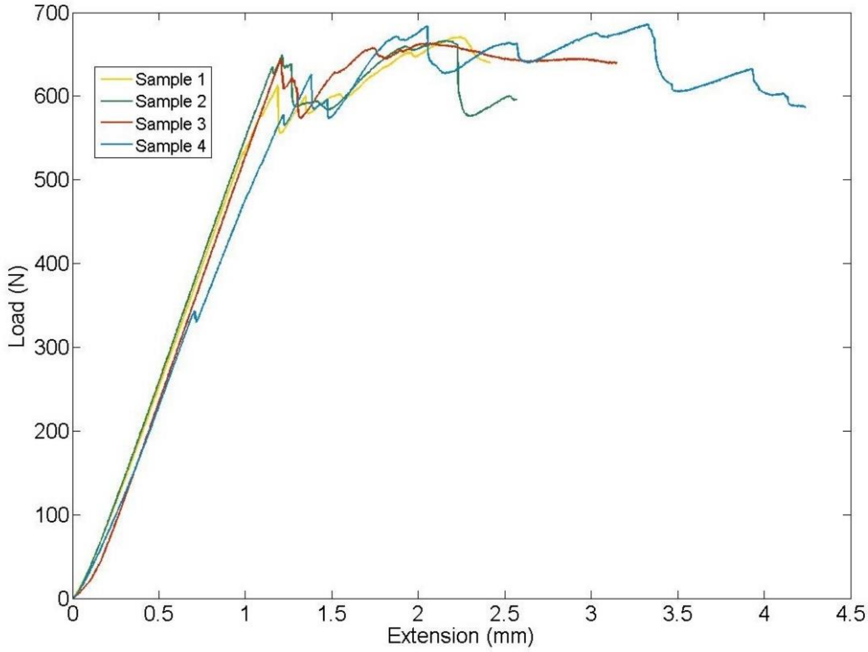

Figure 6-10 Loading curves of Alteco samples.

All four samples displayed similar behaviors when subjected to the loading condition of the three-point bending test set-up. The results of the samples showed consistency in maximum load, stiffness and failure mode. The samples failed progressively during the testing process. Further examination of the tested samples showed rupture of the top CFRP ply due to compression. No failure of the ABS material was observed in any of the samples. Individual Load – Extension curves of samples can be found in Appendix B.

6.2. Bending test of L-shaped samples

6.2.1. Bare L-shaped samples

3D printed L-shaped samples with I-shaped cross section (one face-up and one edge-up) were tested with the bending test setup.

Table 6-9 Bare ABS L-shaped samples' measurements.

Sample	Configuration	Weight (g)
1	Face-up	38.58
2	Edge-up	38.04

Table 6-10 Bare ABS L-shaped samples' bending test results.

Sample	Max Load (N)	Extension at max load (mm)	Flexural Stiffness Coefficient (N/mm)
1	59.314	25.56	4.611
2	39.051	11.56	3.967

The face-up sample had multiple small failures in the structure until a large fracture occurred at the clamped position. The edge-up sample fails at the joint between the long leg and the short leg of the sample. Individual Load – Extension curves of samples can be found in Appendix B.

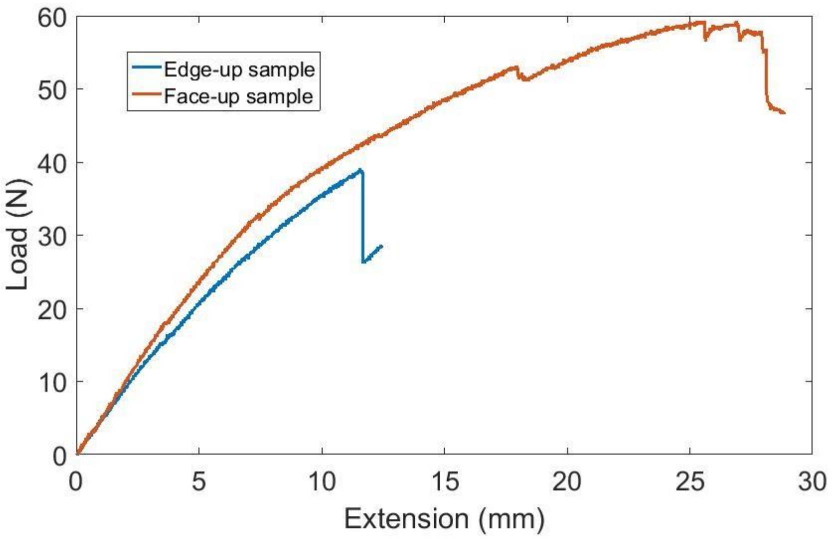

Figure 6-11 Loading curves of bare ABS L-shaped samples.

6.2.2. CFRP Reinforced L-shaped samples

Four samples (two face-ups and two edge-ups) were reinforced with CFRP and Alteco Cyanoacrylate adhesive and tested with the bending test setup. Individual Load – Extension curves of samples can be found in Appendix.

Table 6-11 CFRP reinforced L-shaped samples' measurements.

Sample	Configuration	Weight (g)	Percentage increase in weight
1	Face-up	40.5776	4.42
2	Face-up	40.4203	4.07
3	Edge-up	39.7343	4.81
4	Edge-up	39.8097	4.38

Table 6-12 CFRP reinforced L-shaped samples' bending test results.

Sample	Load at first failure(N)	Extension at first failure (mm)	Flexural Stiffness Coefficient (N/mm)
1	34.033	7.184	5.01
2	36.005	7.408	5.17
3	41.269	9.659	4.93
4	55.83	19.975	3.77

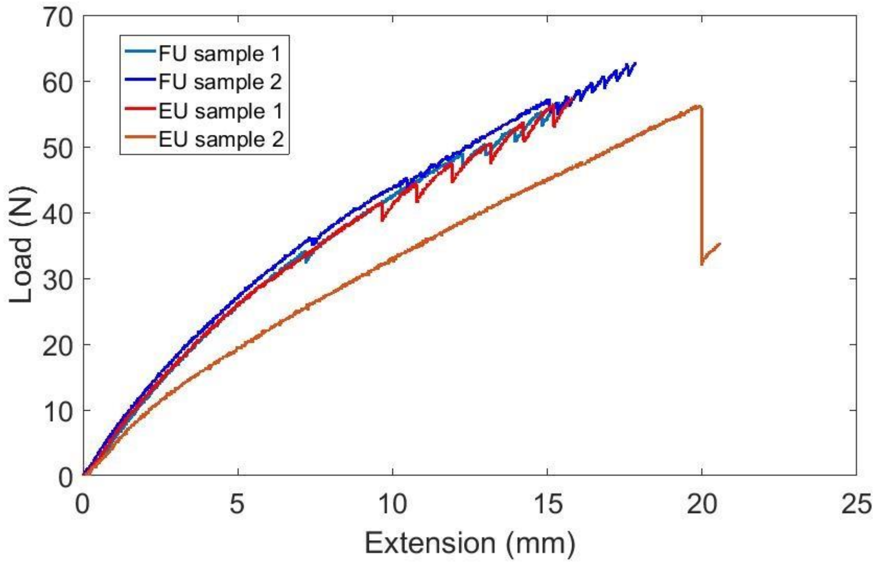

Figure 6-12 Loading curves of CFRP reinforced L-shaped samples.

Sample 1, 2, and 3 show small progressive failures. In all cases, no damage in the CFRP or adhesive debonding was observed. The progressive failures were likely to have happened in the ABS. For sample number 4, there was no sign of progressive failure, the sample failed when a crack was formed at the joint between the long leg and the short leg of the sample, similarly to the bare edge-up sample.

6.2.3. Fill compositing L-shaped samples

Four samples (one face-up and three edge-up) were reinforced with Epolam 5051 epoxy resin and tested with the bending test setup. Samples measurements and results are shown below. Individual Load – Extension curves of samples can be found in Appendix B.

Table 6-13 Fill compositing L-shaped samples' measurements.

Sample	Configuration	Weight (g)	Percentage increase in weight
1	Face-up	108.257	179
2	Edge-up	106.243	179
3	Edge-up	110.294	190
4	Edge-up	112.92	196

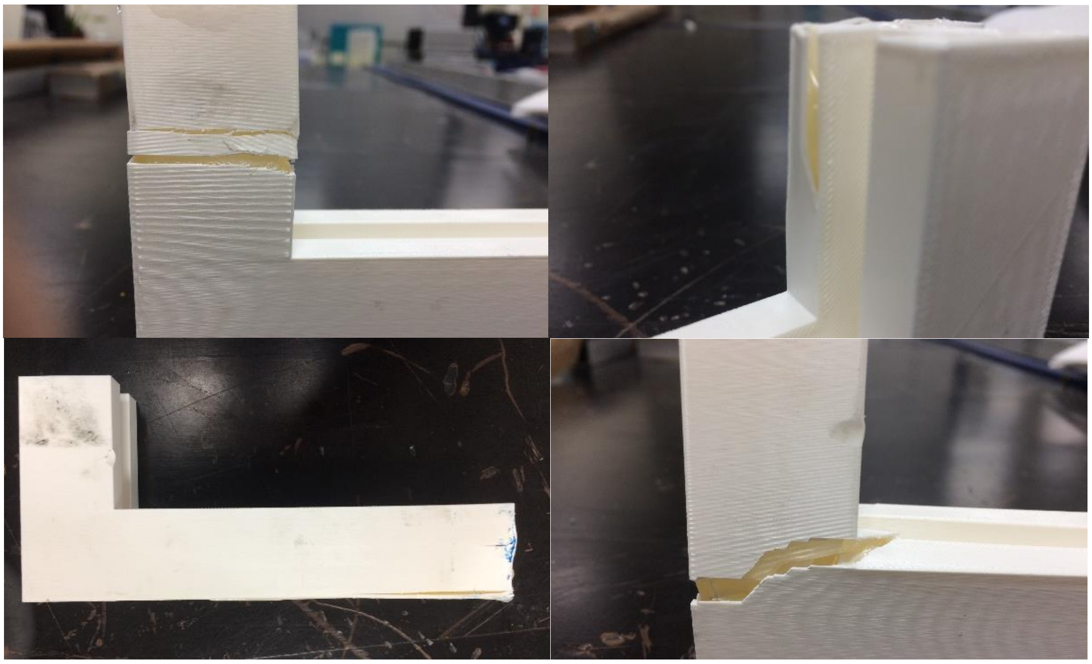

Figure 6-13 Fractures of fill compositing samples post-test.

Table 6-14 Fill compositing L-shaped samples' bending test results.

Sample	Max Load (N)	Extension at max load (N)	Flexural Stiffness Coefficient (N/mm)
1	414.406	19.942	29.38
2	504.911	25.791	32.7
3	844.713	22.817	51.97
4	701.293	30.425	32.46

There were large increases in weight for all samples with the addition of the fill compositing material. The four fill compositing samples showed similar behavior in the Hookean region. All samples had fractures in both the ABS material and the Epolam filling. The position of failures varied for each sample as shown in Figure 6-13. Under loading, the fill composite helped to retain the shape of the ABS as opposed to the CFRP reinforcing on the top and bottom surfaces. Stiffness and maximum load of the fill compositing increase significantly.

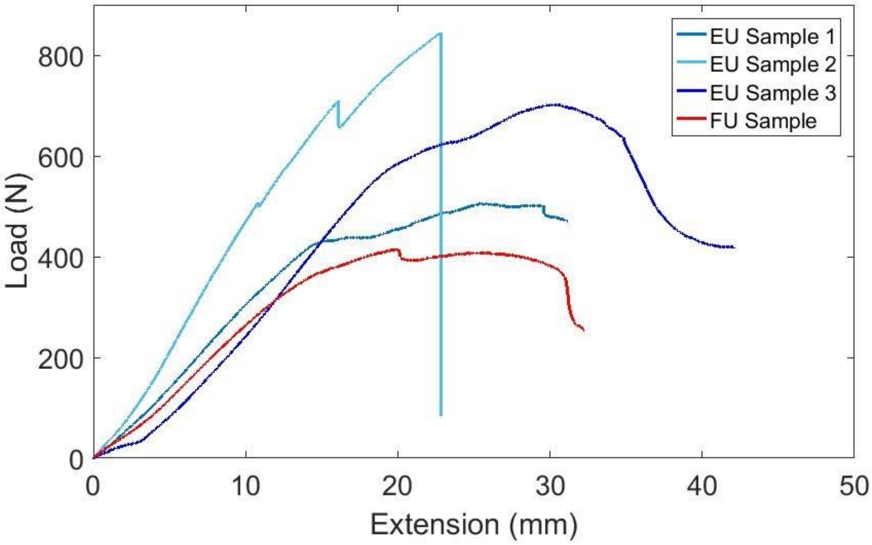

Figure 6-14 Loading curves of fill compositing L-shaped samples

6.3. Motor arm sample

A solid motor arm was reinforced with CFRP and Alteco Cyanoacrylate adhesive and tested with a bending test setup. The load was applied at the motor mount position and the arm was placed upside down so that the load simulated the loading direction in actual flight. The descending rate for the loading nose was 0.5mm/min.

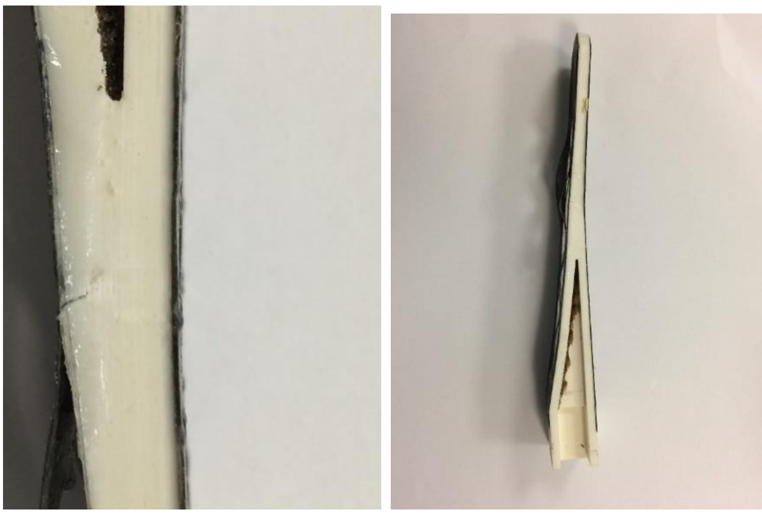

Figure 6-15 Post-test motor arm reinforced with CFRP. Debonding and fractures in the ABS material can be observed.

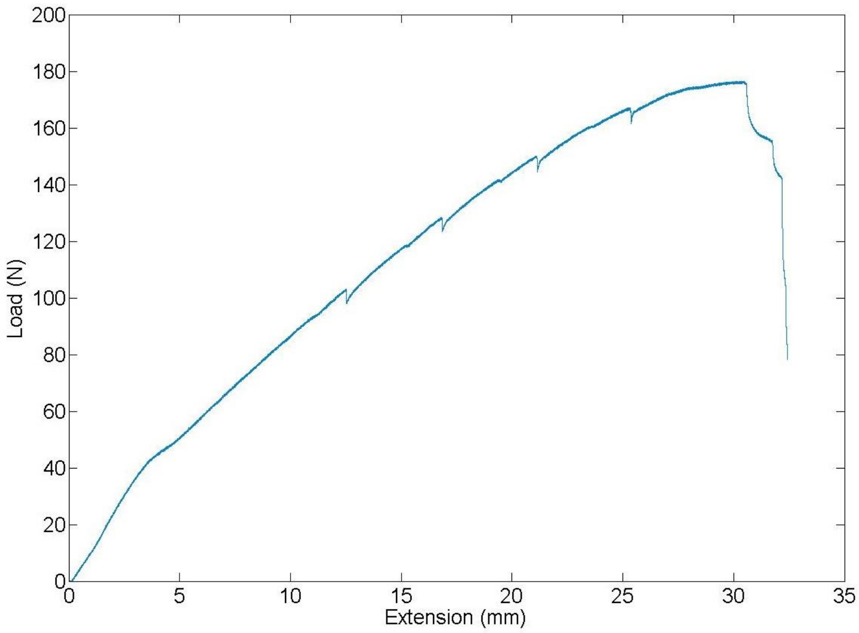

Figure 6-16 Loading curve of CFRP reinforced motor arm.

The motor arm had multiple progressive failures. The first minor failure occurred at the load of 102.25N at 12.54mm extension. The max load of the motor arm was 176.46N at 30.07mm. The flexural stiffness coefficient before failure is 7.23 (N/mm).

During the test, minor failures in the ABS and debonding of the adhesive occurred causing small sudden drops in loading. There was no visible fracture on the CFRP but fractures in the ABS was observed to caused large drops in the loading that the arm can take.

7. TOPOLOGY OPTIMIZATION

Topology optimization can be done in the design phase. By doing topology optimization, the effectiveness of the design can be improved since it allows the removal of excess material which does not contribute the strength of the part, thus creating an optimized structure for the designed load.

For the L-shaped sample with I-shape cross-section, topology optimization was done to improve the geometry of the structure to optimize for the loading of the bending test. Hypermesh software was used to optimize the sample in this project. The procedure is as followed:

1. A model of the L-shape sample was imported as a STEP file. For the optimization process in this project, a solid model without inner channels was used.
2. Create and input the material properties of ABS. Assign the material to the model.
3. Create a mesh for the model.
4. Create nodes for boundary conditions and loads.
5. Apply the boundary conditions by adding constraints to the selected nodes.
6. Apply and transfer the loads to respective nodes.
7. Create load step.
8. Run OptiStruct analysis.
9. View result to get the contour plot of stresses on the model.
10. Set response, constraints, objective reference, objective, and run option for optimization
11. If the optimization is successful, the final iteration in the result would show the optimized model, which can be saved as an STL file.
12. Refine the optimize model by smoothening its surface. This can be done with other software, such as solidThinking Inspire.

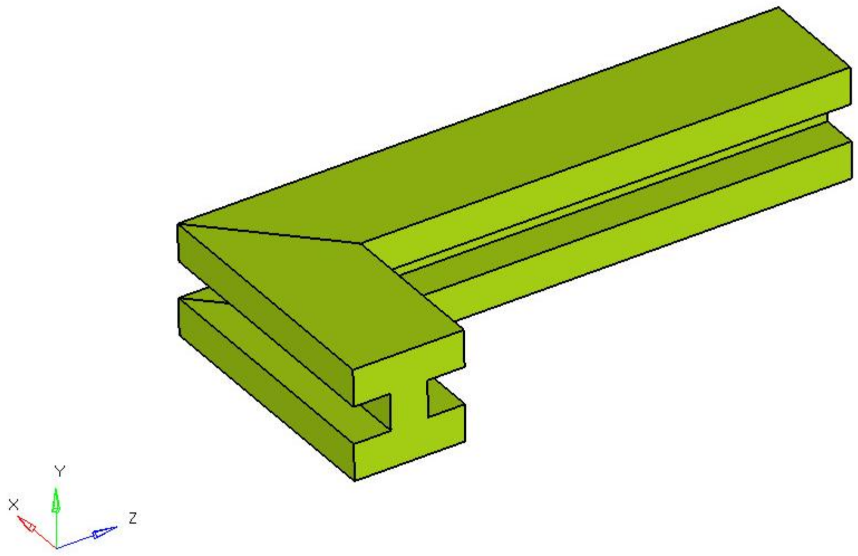

Figure 7-1 Solid model inputted in the optimization software.

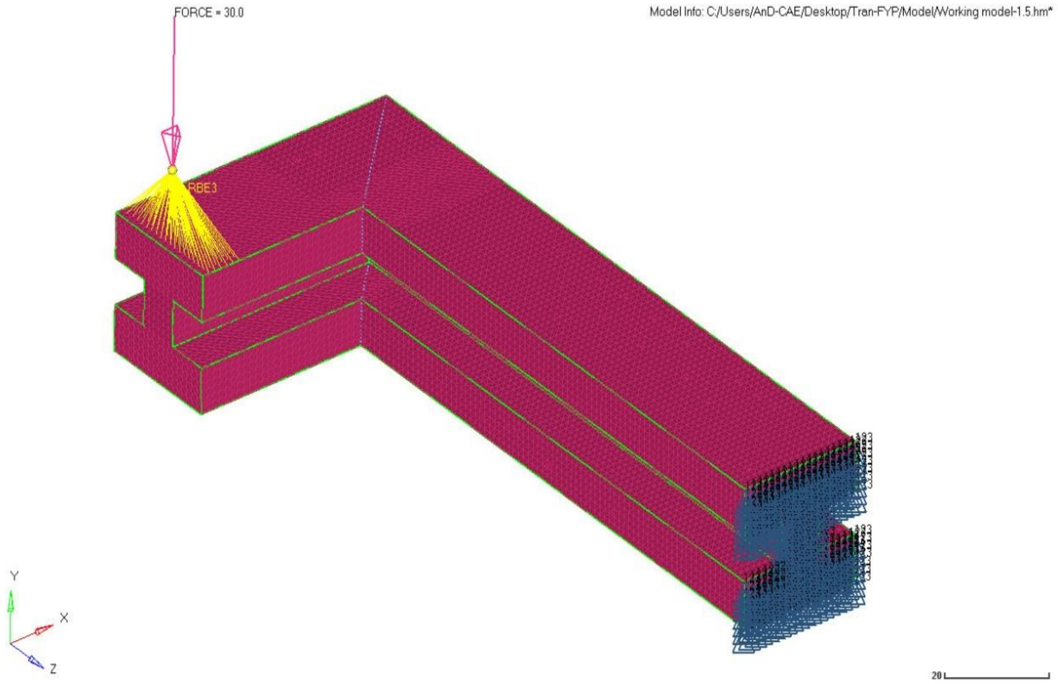

Figure 7-2 Model after meshing and applying boundary conditions and loads.

Mesh size of the model must be carefully considered. Finer mesh would generate more reliable results, but at the same time would require more processing time. The software would determine the optimum element density.

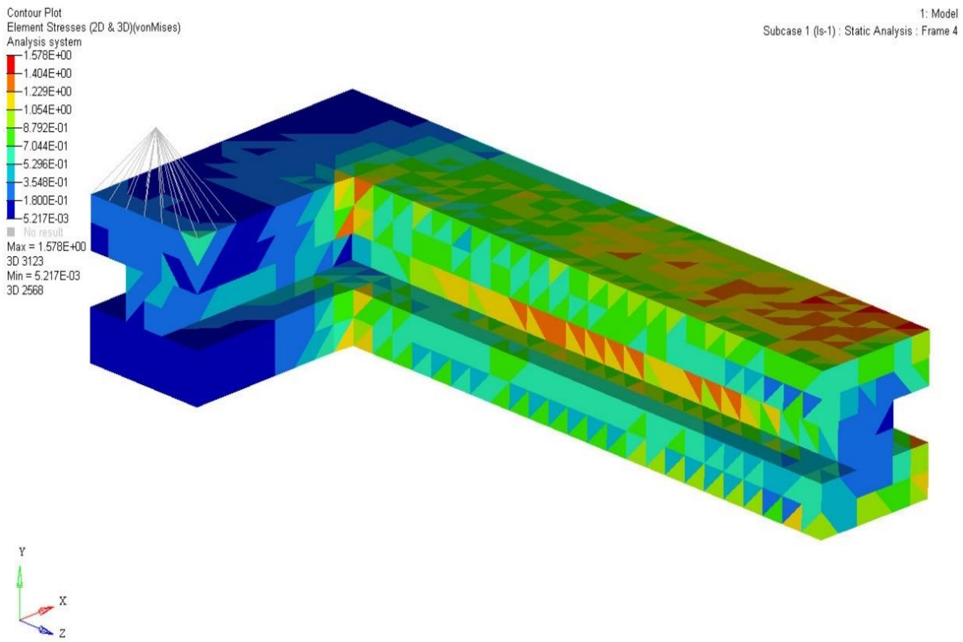

Figure 7-3 Contour plot for model with mesh size of 5.

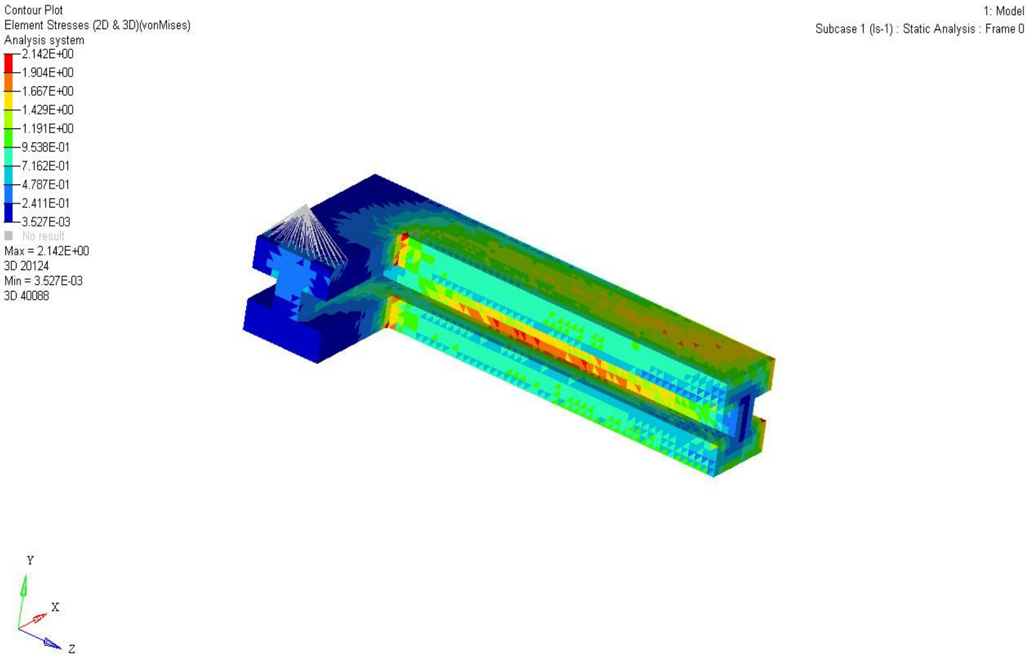

Figure 7-4 Contour plot for model with mesh size of 2.5.

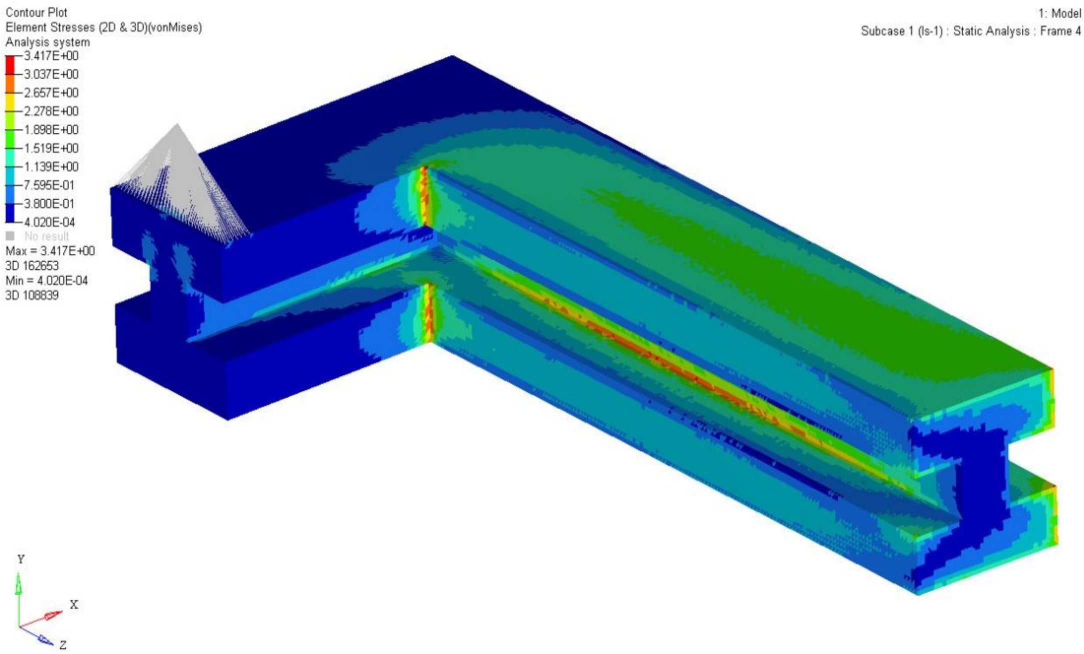

Figure 7-5 Contour plot for model with mesh size of 0.8.

By adjusting the mass fraction, elements with low stresses would be removed. The remaining element would form the optimized structure for the specified loading.

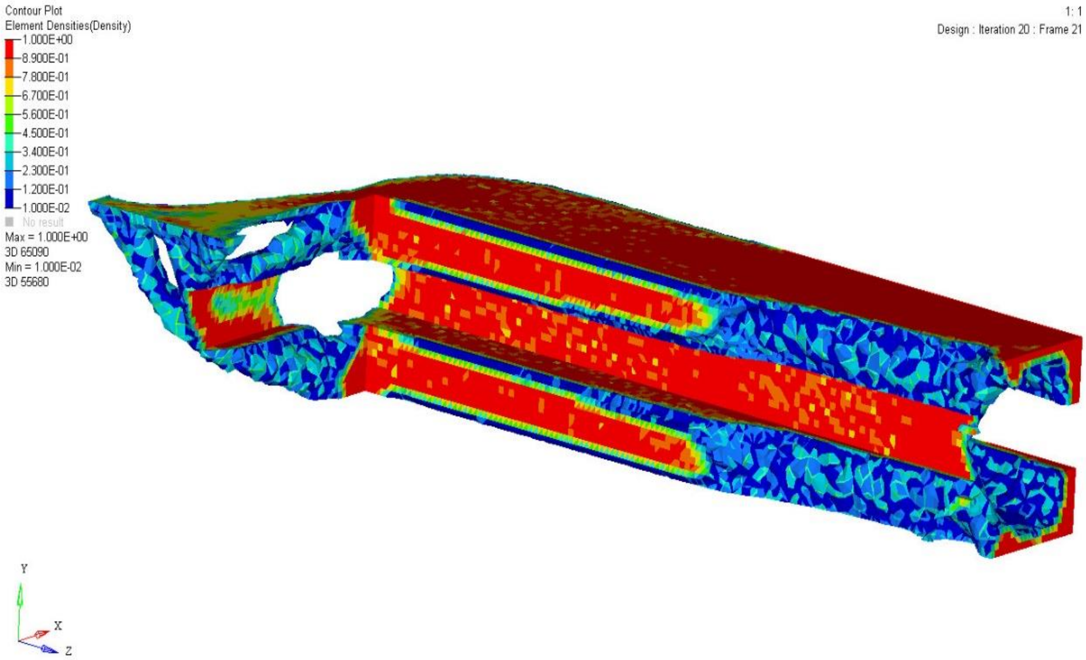

Figure 7-6 Optimized structure obtained at the end of the process.

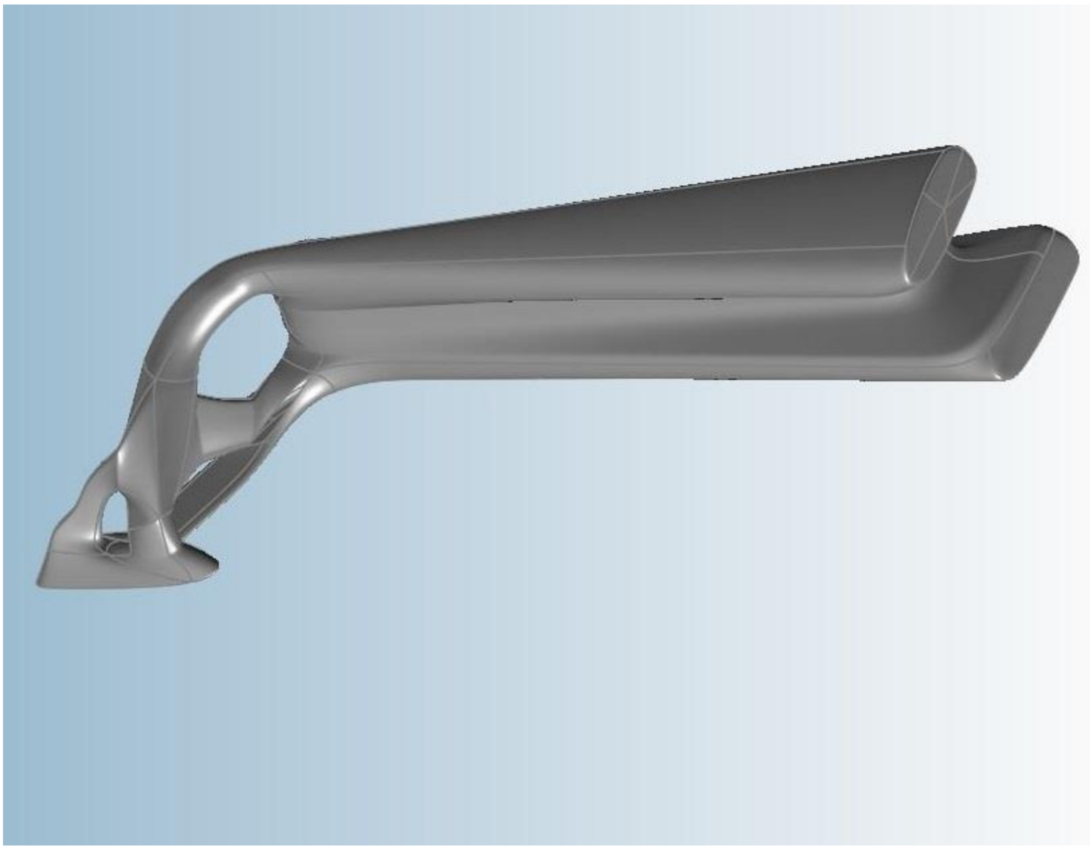

Figure 7-7 Optimized part after being smoothened.

8. DISCUSSION AND RECOMMENDATION

8.1. Discussion

8.1.1. Printed bare ABS

For bare ABS rectangular cross section samples, the three-point bending shows that there is a difference in parameterized flexural stiffness between edge-up and face-up samples. The edge-up samples had higher parameterized flexural stiffness (0.809-0,837 N/mm^4) compared to that of the face-up (0.722-0.774 N/mm^4). However, as the results from the experiment showed, the difference in the parameterized flexural stiffness was offset by the difference in thickness. All samples had similar load-extension curves in the elastic region, and also part of the plastic deformation (from 0 to 6mm extension). This suggests that the orientation of the ABS printed part would have little effect on the results of three-point bending tests of CFRP strengthening samples, which had extensions of less than 4mm.

8.1.2. CFRP Strengthening of three-point bending samples

Three types of adhesive were used to apply CFRP to ABS samples: Redux 335K adhesive, Araldite epoxy, and Alteco Cyanoacrylate adhesive. Some of the key results are listed below (percentage increase in weight, maximum load, and parameterized flexural stiffness values are the averages of the samples tested):

Table 8-1 Percentage increase in weight, max load, parameterized flexural stiffness, and deviations for bare ABS and CFRP reinforced three-point bending samples.

Material	Percentage increase in weight	Max load (N)	Max Load standard deviation	Parameterized Flexural Stiffness (N/mm^4)	Parameterized Flexural Stiffness standard deviation
Bare ABS	0	99.06	0.93%	0.781	6.06%
Redux Samples	41.4%	399.74	44.4%	8.48	9.48%
Araldite Samples	33.8%	510.91	15.2%	8.28	4.62%
Alteco Samples	34.4%	671.48	1.48%	8.66	6.30%

All samples showed significant an increase in flexural stiffness and maximum load. The average parameterized flexural stiffness (as calculated in section 5.1) of each type of reinforced samples ranged from 8.28 to 8.66 N/mm^4 compared to the average stiffness parameterized flexural stiffness of 0.781 N/mm^4 of the bare samples. The flexural stiffness values of the reinforced samples were comparable. This might be explained by the positioning of the reinforce material, which was on the top and bottom surface of the sample, where the sample experience the most stress. Thus, the consistency in the flexural behavior of the sample in the Hookean region was because the CFRP would take most of the stress when the sample is bent.

For maximum loading, the samples with Alteco adhesive performed the best, achieving consistent results in load, stiffness, and mode of failure. Redux samples have the lowest load capacity and the highest deviation. However, it should be noted that the Redux sample which failed by CFRP rupture had a comparable maximum load with that of the Alteco samples. The Araldite, on the other hand, despite being consistent, could not reach the same maximum load attained with CFRP rupture since all the Araldite samples failed by debonding of the adhesive layer. The lack of chemical reaction between ABS and epoxy caused poor adhesion between the CFRP and ABS. It can be concluded that the mode of failure is vital in determining the maximum load that the sample can support. This can be observed in Figure 6-4. For the same adhesive, the sample failed by CFRP rupture has much higher maximum loading compared to that of the samples failed by debonding. CFRP rupture is the desired mode of failure to maximize the load capacity of the reinforced part.

Of the three adhesives chosen for testing the CFRP reinforcement method, Alteco Cyanoacrylate adhesive was the best performer with a good combination of factors including the increase in weight, loading, and flexural stiffness.

8.1.3. Bending test of L-shaped samples

Bare ABS, CFRP reinforced and fill compositing L-shape samples were subjected to bending tests to evaluate the performance of reinforcement methods in more complex settings. Below are some of the results and measurements from the bending tests:

Table 8-2 Percentage increase in weight, max load, flexural stiffness bare ABS, CFRP reinforced, and fill compositing L-shaped samples.

Material	Percentage increase in weight	Stiffness Coefficient (N/mm)	Stiffness Coefficient Standard Deviation (%)
Bare ABS	0	4.29	10.62
CFRP reinforced ABS with Alteco adhesive	4.42%	4.72	13.58
Fill compositing ABS with Epolam	186%	36.63	28.23

In this bending test, we see that the orientation of the printing had an effect on the performance of the samples. For the edge-up samples, the planes of the printing layers were parallel to the loading direction, which made the samples more prone to fail due to the fractures originated between the layers.

Despite this variation between the two orientation, there were certain trends that were observed throughout the tests. First, there was an increase to stiffness coefficients for both types of reinforcement. The CFRP method produced a minor improvement to the stiffness of the samples while adding little weight. On the other hand, fill compositing method increased the weight of the samples by nearly 200%, but also significantly increased their stiffness. From observation during the test, this could be contributed to the degree at which each method can sustain the integrity of the main ABS structure. Samples which can maintain its form when put under load would perform better and have higher stiffness value. Therefore, the fill compositing method, which fills the samples with material with higher strength, show a much higher increase in stiffness compared to that of the CFRP reinforced samples, which only increase the stiffness at the top and bottom surface.

The deviations in the results for the bending test can be alleviated with further improvements in the designs of both the samples and the experimental setup. This should be a focus in future study.

8.1.4. Topology optimization

Topology optimization was applied to the L-shaped samples under the loading condition of the bending test. The results showed the stress distribution among the elements. From this distribution of stress, the design was optimized by eliminating the elements where there was low or no stress. With this, a design with lower volume was obtained. The more efficient design would enable more saving on material used for fabrication.

However, it should be noted that the optimized design had a much more complex structure compared to that of the original design as the removing of elements forms holes and void in the structure. Therefore, fabricating the optimized parts should be done with 3D printing instead of conventional manufacturing methods.

8.2. Recommendations

For CFRP reinforcement, since adhesion between the plays a vital role in determining the stiffness and maximum load of the samples, improving adhesion would yield better results. This can be done by refining the procedure for sample preparation or choosing different types of adhesive. Specifically, Alteco cyanoacrylate adhesive has a very low set time of under one minute. While it was possible to properly apply the CFRP to the three-point bending samples and the L-shaped samples, larger samples with more complex surfaces such as the motor arm requires the adhesive and CFRP to be applied segment by segment. This might be one of the principal causes leading to poor adhesion between to two materials. Furthermore, the adhesion can be improved by implementing a surface preparation process for the samples before applying the adhesive.

Designs for fill compositing samples should be more compatible with the method. A mold-like inner structure should be employed to prevent leaking as well as the forming of voids and bubble in the samples. The material for fill compositing should have low enough viscosity and sufficient gel time and set time so that the filling process is possible.

Designs for bending test should also be altered to limit the discrepancies of the testing conditions. Samples should be designs in such a way that secure and consistent clamping can be done with current setup. This will vastly improve the consistency of the results obtained from the tests.

9. CONCLUSION

Two methods of reinforcing 3D printed ABS plastic bags were studied: CFRP reinforcement and fill compositing. All samples were printed by Stratasys Dimension Elite 3D printing machine using ABS-plus P430. The CFRP used primarily was AX-6200-C from Axiom Materials. Adhesives used for CFRP reinforcement included Redux 335K, Araldite standard epoxy, and Alteco Superglue 110 Cyanoacrylate adhesive.

Only bending tests were done to study fill compositing while CFRP reinforcement was also tested with three-point bending and on a real UAV motor arm. The three-point bending tests were done in accordance with ASTM D790 standard, where the span was 50 mm, width was 12.7 mm and design depth of ABS is 3.2 mm. For both methods, control tests were done with bare ABS material to determine the improvement attained by reinforcing.

CFRP strengthening showed positive results for all three types of adhesive. CFRP reinforced samples have parameterized flexural stiffness more than 10 times higher than that of bare ABS. However, it should be noted that the mode of failure is vital to the overall performance of the reinforcement. Through the experiment, it was found that the desirable mode of failure is CFRP rupture, where the CFRP would take on most of the loading applied to the structure. Therefore, Alteco cyanoacrylate adhesive was determined to be the best adhesive of the three for CFRP strengthening as it showed the consistency in bonding ABS to CFRP material, thus increase the flexural stiffness of the sample.

Fill compositing method can also greatly increase the performance of samples in both load and stiffness. However, there were large deviations in the results. Hence, utilizing the method would require more consideration in the design phase to achieve more consistency.

Knowing the loading condition on each part can also allow optimization to be made in the design phase. This is done by using topology optimization, which can make lighter parts that are designed specifically to perform under prescribed conditions. The method should help save material as well as providing insight on how to utilize other methods of strengthening.

Apply the two methods on UAV would be possible, and there are pros and cons to each method. Compare to fill composting, CFRP reinforcement requires a much lower increase in weight, but it can only be in the form of an attachment to the exterior of the parts. Thus, while CFRP reinforcement would suits well with simple parts with flat surfaces or thin walled structure, parts with complicated structures and surfaces would not be compatible with the methods. On the other hand, more complicated parts may work to the advantage of fill composting method since it offers more versatility in designs. However, weight and complex procedures must be taken into account.

10. FUTURE STUDIES

Future research could be done with more variations to the tests carried out in this project. For three-point bending of CFRP reinforced samples, the depth of ABS samples could be varied to optimize strength to weight. Other configuration, such as having a single CFRP prepreg for reinforcement, or adding more layers of prepreg, can also be considered.

Fill compositing studies can be broadened and improved by testing with different types of resin materials, and refined testing methods and sample preparation. Resins can be further improved by mixing with short fibers and other materials. Other testing methods can be added to diversify the loading conditions.

Topology can be used in the design phase to reduce the amount of printed material as well as serve as a guideline to strengthen the part. The part can be designed so that fill compositing or CFRP reinforcement or both can be added to strengthen positions which the topology optimization states that the material density should be higher.

REFERENCES

1. Gebhardt, A. and J.-S. Hötter, *Additive Manufacturing - 3D Printing for Prototyping and Manufacturing*. Hanser Publishers.
2. Srivatsan, T.S., K. Manigandan, and T.S. Sudarshan, *Additive Manufacturing of Materials: Viable Techniques, Metals, Advances, Advantages, and Applications*, in *Additive Manufacturing*. 2015, CRC Press. p. 1-48.
3. Wong, K.V. and A. Hernandez, *A Review of Additive Manufacturing.* ISRN Mechanical Engineering, 2012. **2012**: p. 1-10.
4. Oh, Y.T. and G.D. Kim, *A benchmark study on rapid prototyping processes and machines: quantitative comparisons of mechanical properties, accuracy, roughness, speed, and material cost.* Proceedings of the Institution of Mechanical Engineers, Part B: Journal of Engineering Manufacture, 2008. **222**(2): p. 201-215.
5. Domingo-Espin, M., et al., *Mechanical property characterization and simulation of fused deposition modeling Polycarbonate parts.* Materials & Design, 2015. **83**: p. 670-677.
6. Gajdoš, I., et al., *Structure and tensile properties evaluation of samples produced by Fused Deposition Modeling.* Open Engineering, 2016. **6**(1).
7. Bagsik, A., et al., *Mechanical analysis of lightweight constructions manufactured with fused deposition modeling.* 2014: p. 696-701.
8. Sung Hoon, A., et al., *Anisotropic Tensile Failure Model of Rapid Prototyping Parts - Fused Deposition Modeling (FDM).* International Journal of Modern Physics B: Condensed Matter Physics; Statistical Physics; Applied Physics, 2003. **17**(8/9): p. 1510.
9. Chung, D.D.L., *Carbon Fiber Composites*. Elsevier.
10. Park, S.-J., *Carbon Fibers*. Springer Series in Materials Science. 2015.
11. Quinn, K.T., *Shear Strengthening of Reinforced Concrete Beams with Carbon Fiber Reinforced Polymer (CFRP) and Improved Anchor Details*, in *Faculty of the Graduate School of The University of Texas at Austin*. 2009, The University of Texas at Austin. p. 272.
12. Bajpai, P., *Update on Carbon Fibre*. Smithers Rapra Technology.
13. Thanasis, C.T., *Shear Strengthening of Reinforced Concrete Beams Using Epoxy-Bonded FRP Composites.* Structural Journal, 1998. **95**(2): p. 107-115.
14. Teng, J.G., et al., *Behavior of RC Beams Shear Strengthened with Bonded or Unbonded FRP Wraps.* Journal of composites for construction, 2009. **13**(5): p. 394-404.
15. Belter, J.T. and A.M. Dollar, *Strengthening of 3D printed fused deposition manufactured parts using the fill compositing technique.* PLoS One, 2015. **10**(4): p. e0122915.
16. Martin P. Bendsøe, O.S., *Topology Optimization: Theory, Methods, and Applications*. 2004.
17. Chiandussi, G., I. Gaviglio, and A. Ibba, *Topology optimisation of an automotive component without final volume constraint specification.* Advances in Engineering Software, 2004. **35**(10-11): p. 609-617.
18. K. Cai, J.S., *Topology Optimization of a Continuum Structure with Local Volume Constraints*, in *International Conference on Natural Computation*. 2010. p. 3238-3242.

19. Jeong Woo Chang, Y.S.L., *Topology optimization of compressor bracket.* Journal of Mechanical Science and Technology, 2008. **22**: p. 1668~1676.
20. Razvan Cazacu, L.G., *Overview of Structural Topology Optimization Methods for Plane and Solid Structures*, in *Annals of the University of Oradea*. 2014.
21. Tomas Zegard, G.H.P., *Bridging topology optimization and additive manufacturing.* Struct Multidisc Optim, 2015. **53**: p. 175-192.
22. Stratasys, *ABSplus-P430 Data Sheet*. 2014.
23. HEXCEL, *AX-6200-C Data sheet*. 2011.
24. HEXCEL, *Redux 335K Data Sheet*. 2007.
25. Materials, H.A., *Araldite Standard Two component epoxy adhesive Data Sheet*. 2011.
26. ALTECO, *ALTECO SUPERGLUE 110 Data Sheet*.
27. Technologies, A., *Epolam5015 System Data Sheet*. 2008.
28. ASTM, *Standard Test Methods for Flexural Properties of Unreinforced and Reinforced Plastics and Electrical Insulating Materials*. 2015: West Conshohocken, PA.

APPENDIX A

Figure A-1 Dimension Elite FDM machine.

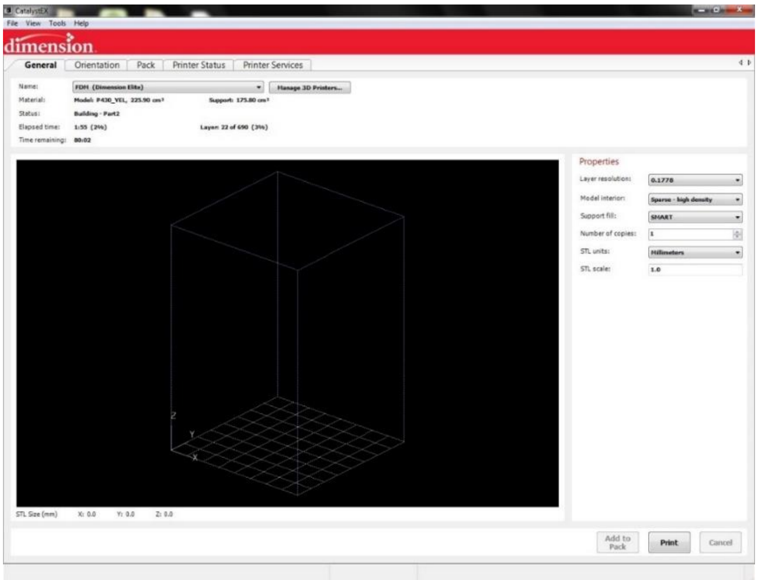

Figure A-2 CatalystEX software main interface.

Figure A-3 Printing plate for Dimension Elite FDM machine.

Figure A-4 SCA-1200 support removal system.

APPENDIX B

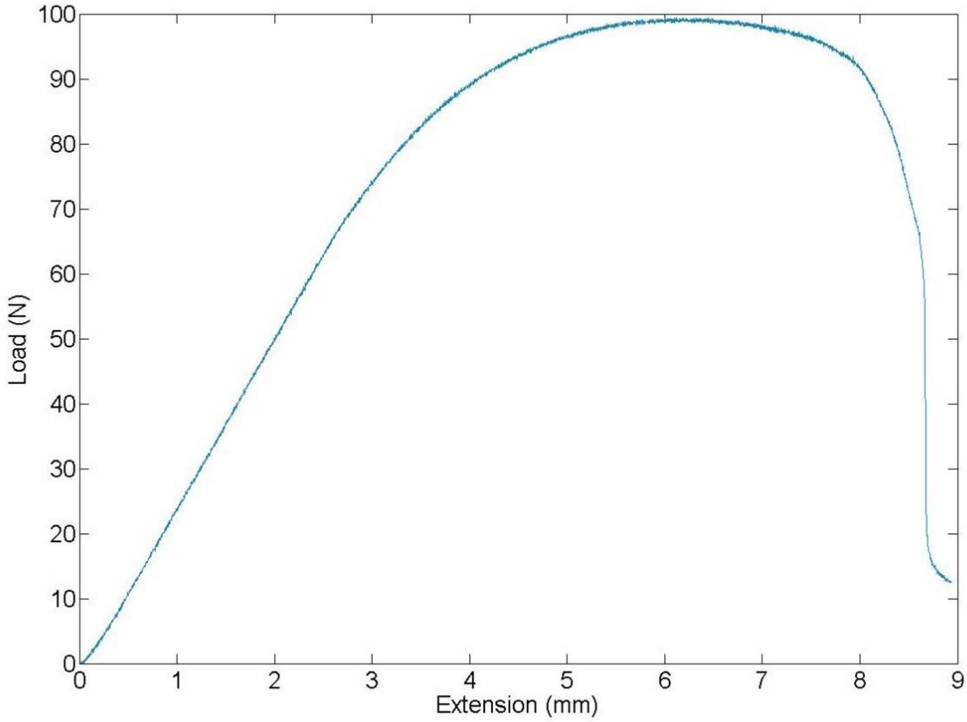

Figure B-1 Loading curve of Bare ABS edge-up sample 1.

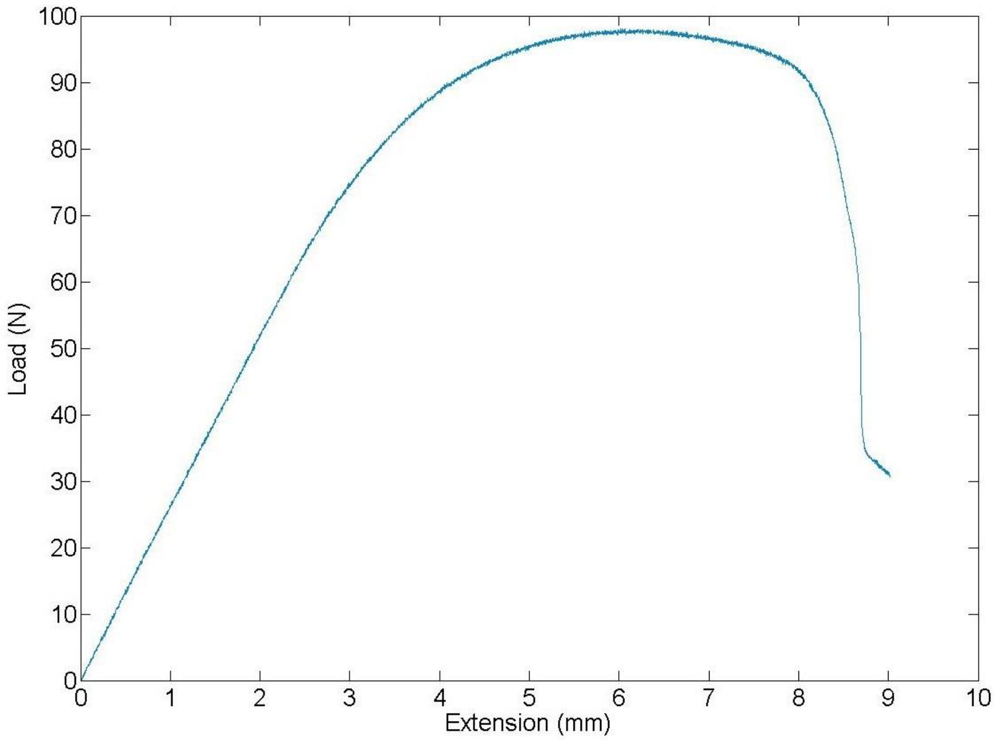

Figure B-2 Loading curve of Bare ABS edge-up sample 2.

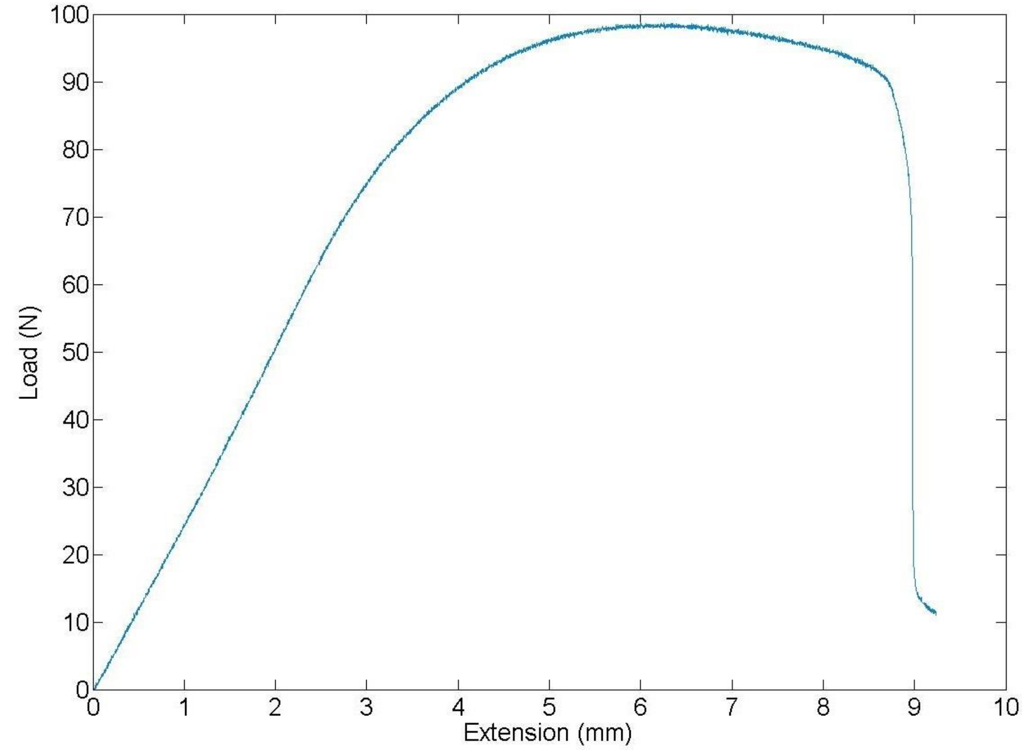

Figure B-3 Loading curve of Bare ABS edge-up sample 3.

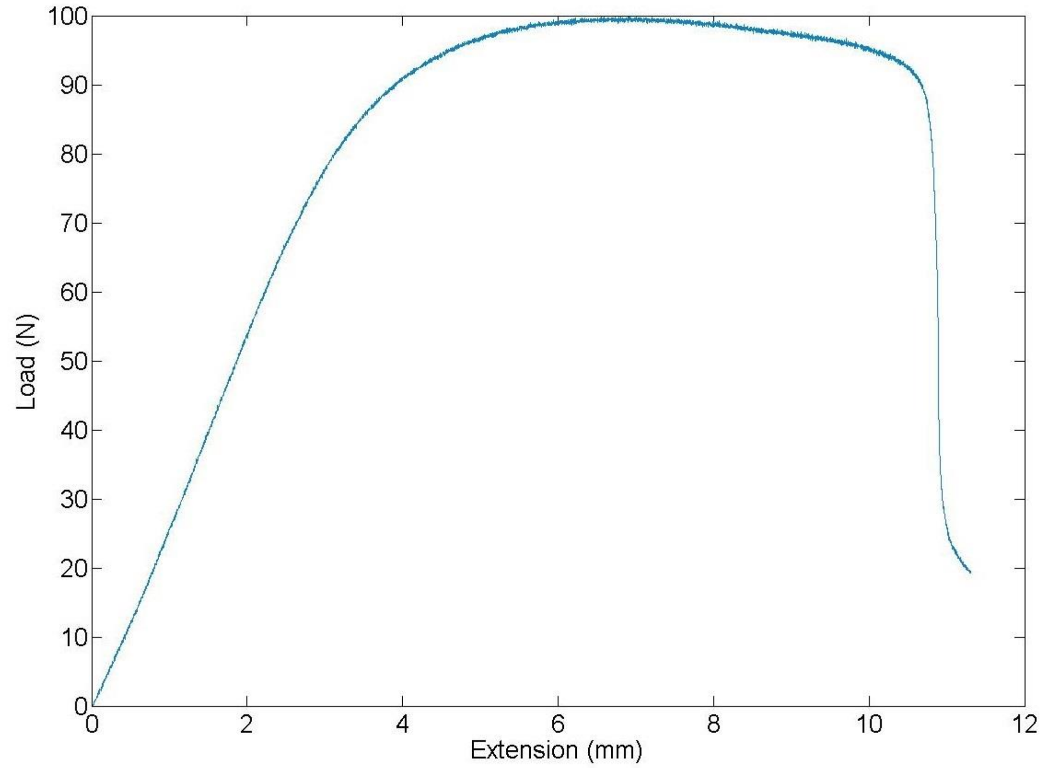

Figure B-4 Loading curve of Bare ABS face-up sample 1.

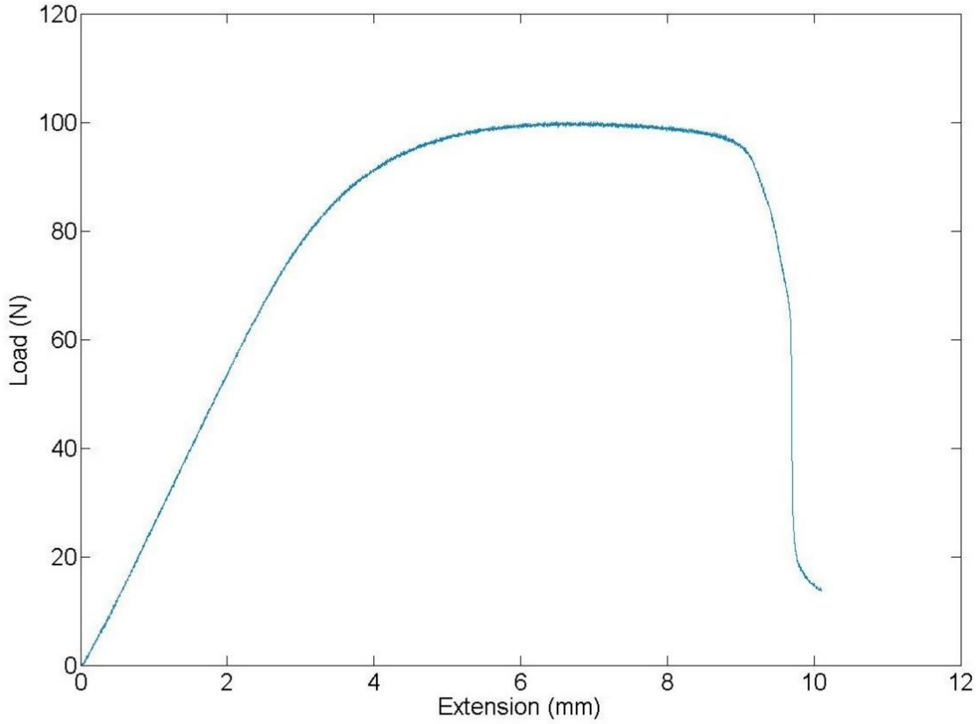

Figure B-5 Loading curve of Bare ABS face-up sample 2.

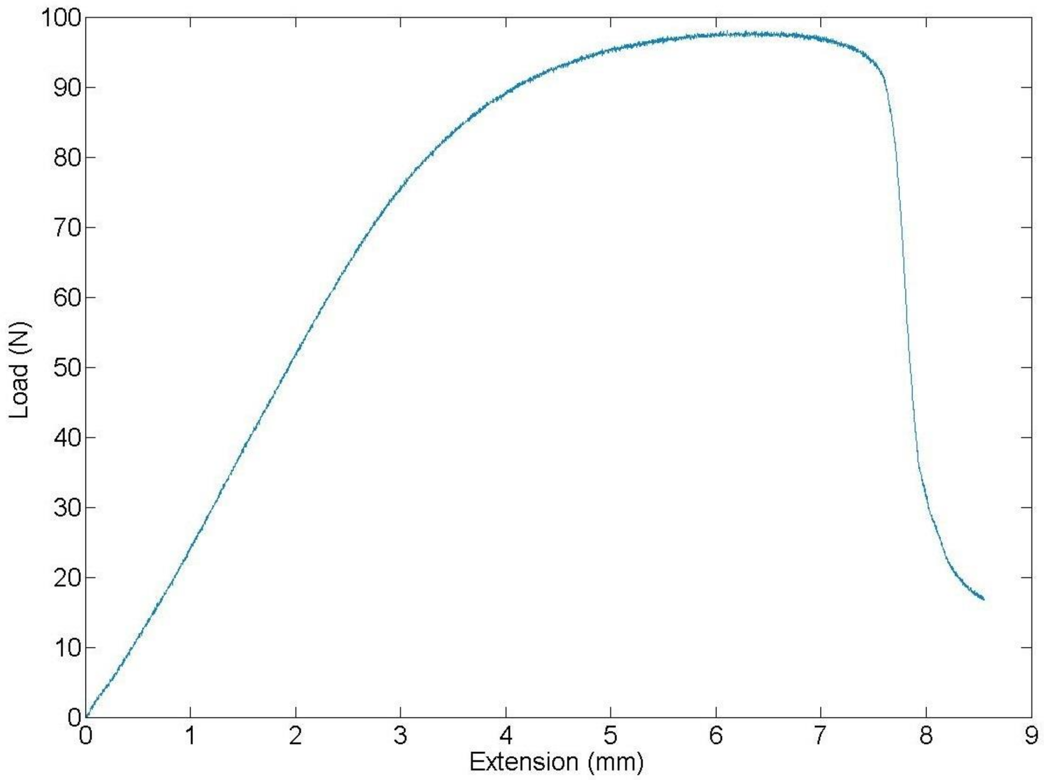

Figure B-6 Loading curve of Bare ABS face-up sample 3.

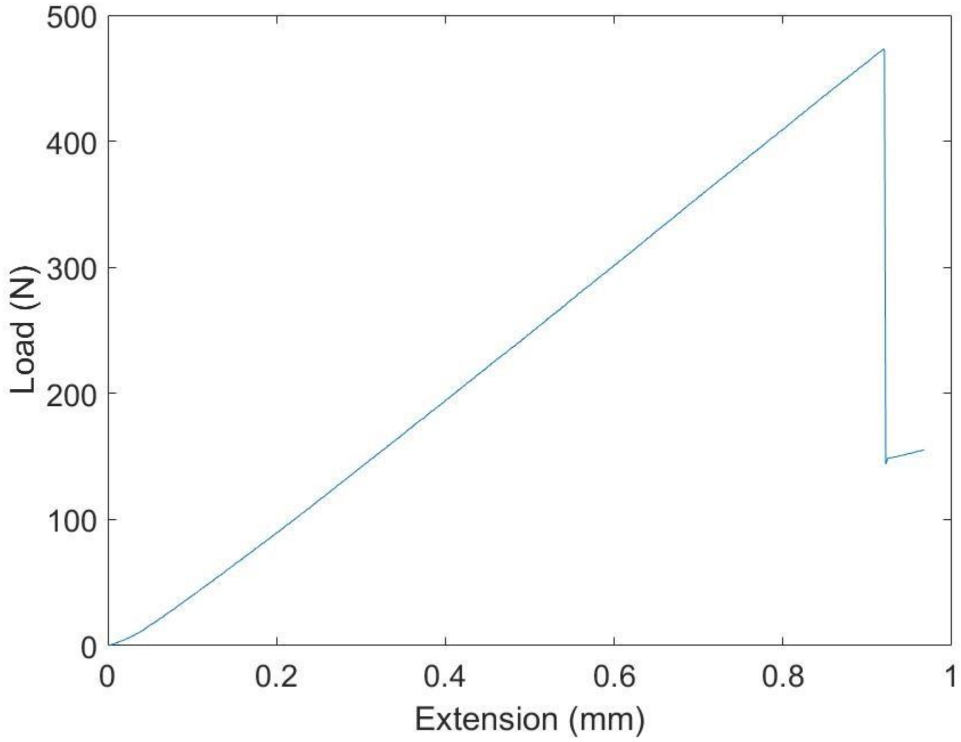

Figure B-7 Loading curve of Araldite sample 1.

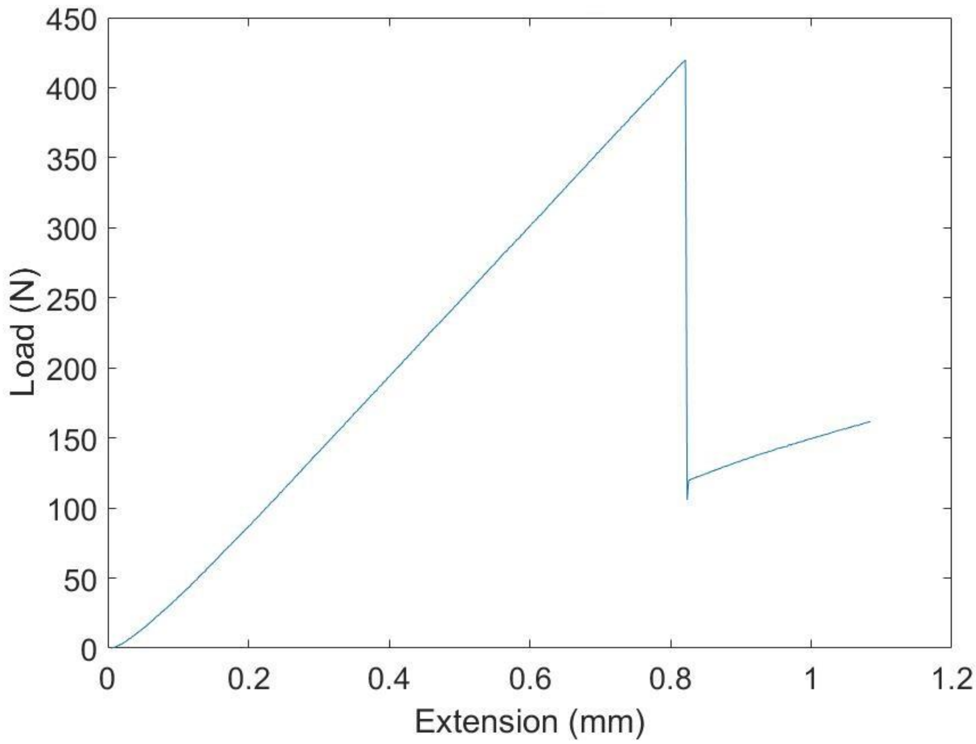

Figure B-8 Loading curve of Araldite sample 2.

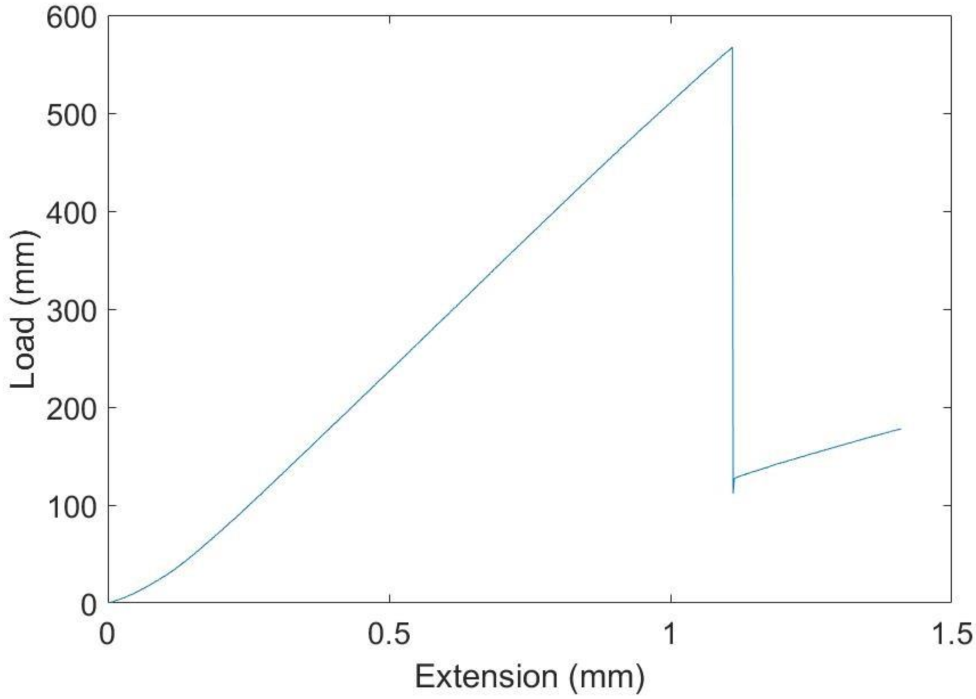

Figure B-9 Loading curve of Araldite sample 3.

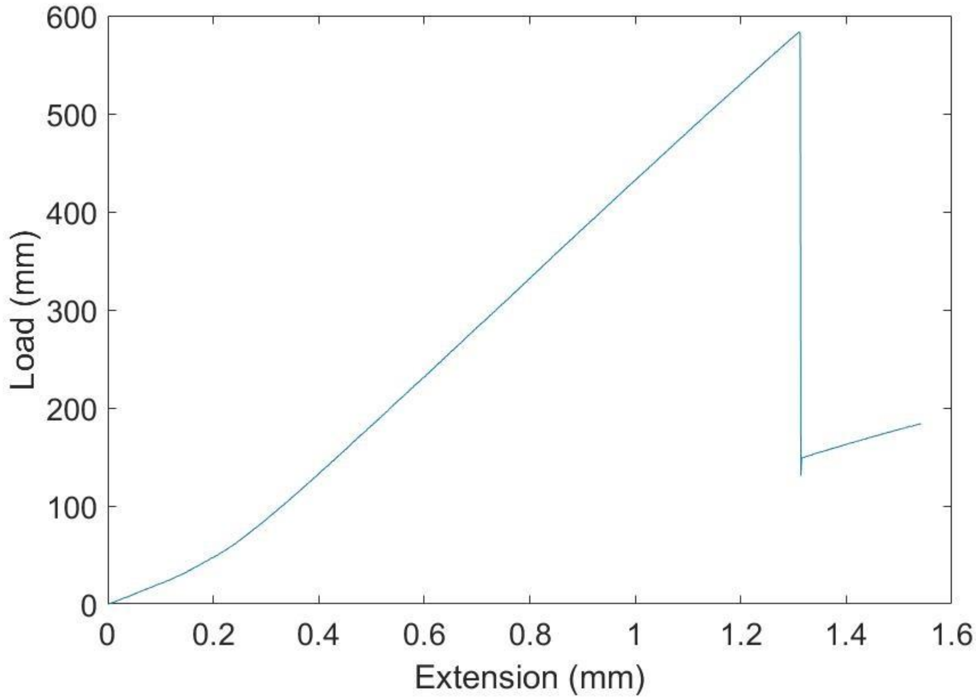

Figure B-10 Loading curve of Araldite sample 4.

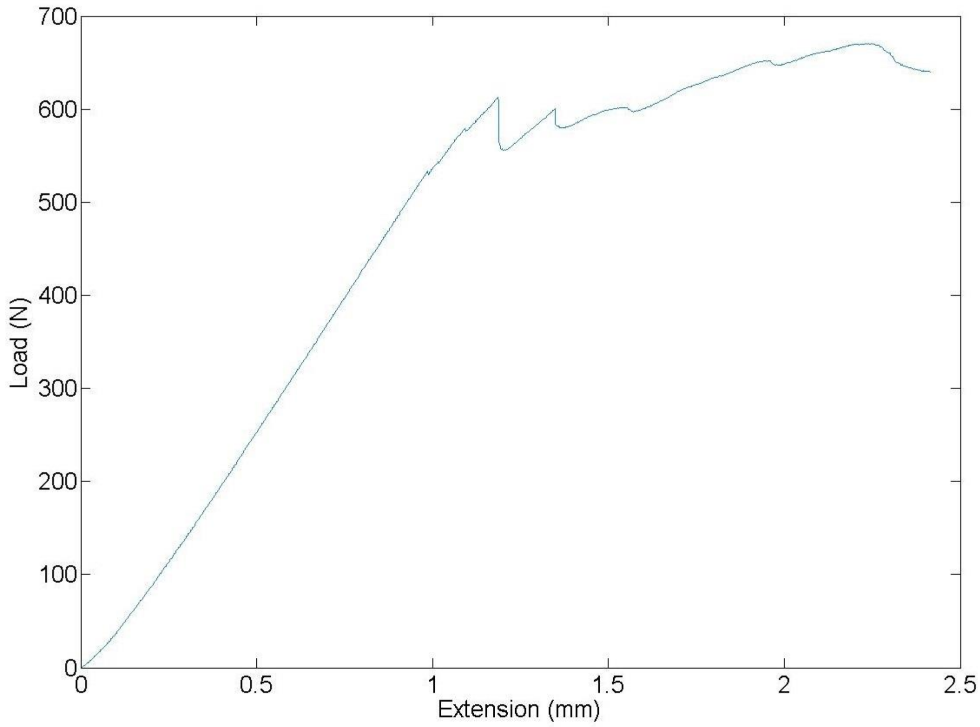

Figure B-11 Loading curve of Alteco sample 1.

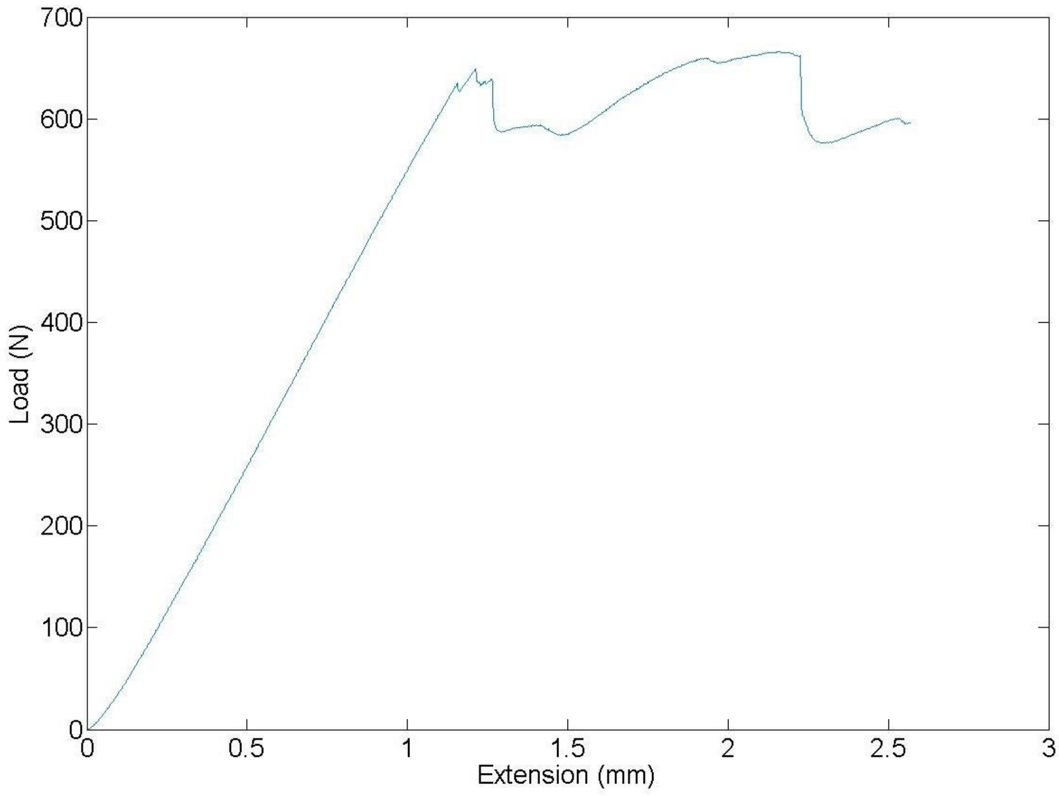

Figure B-12 Loading curve of Alteco sample 2.

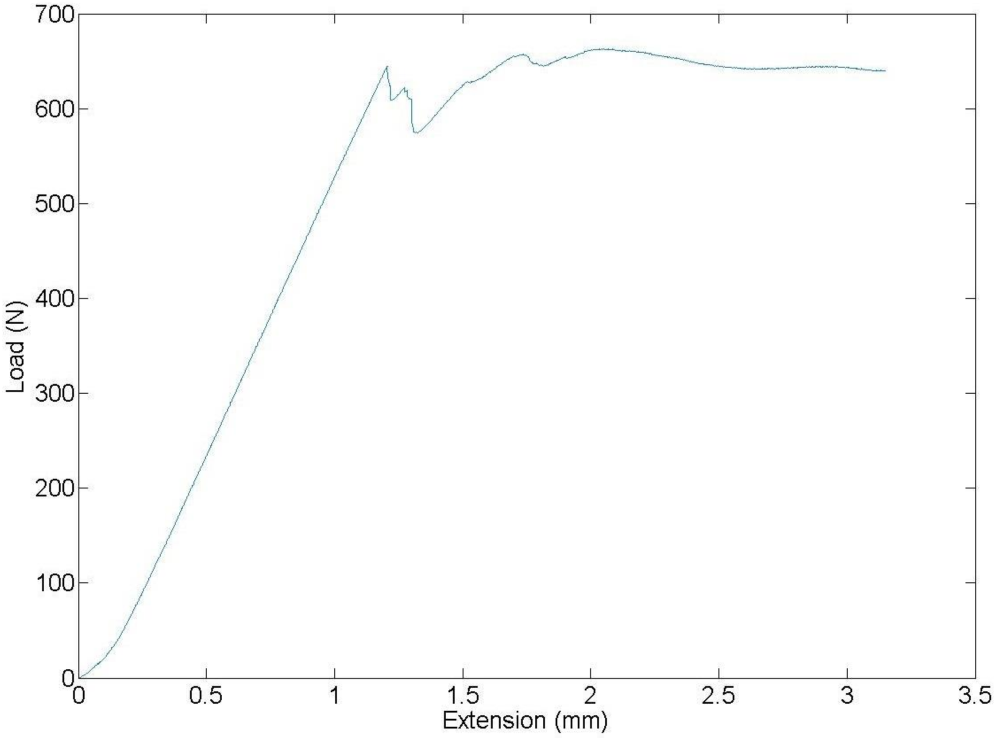

Figure B-13 Loading curve of Alteco sample 3.

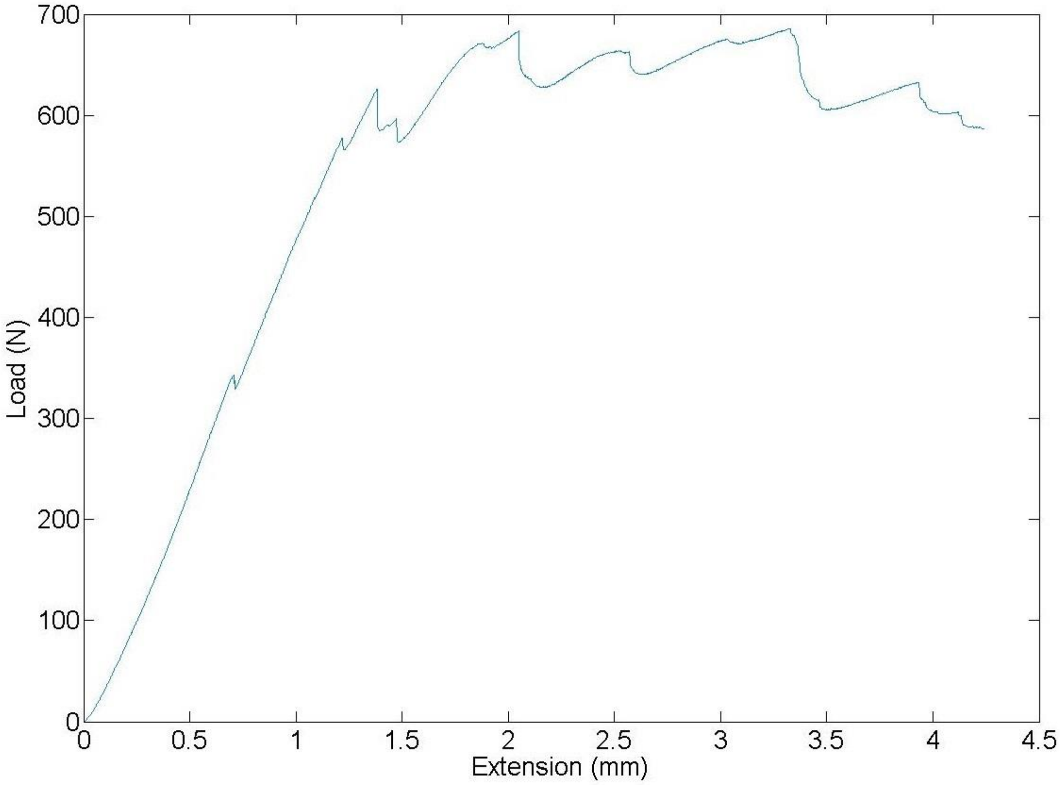

Figure B-14 Loading curve of Alteco sample 4.

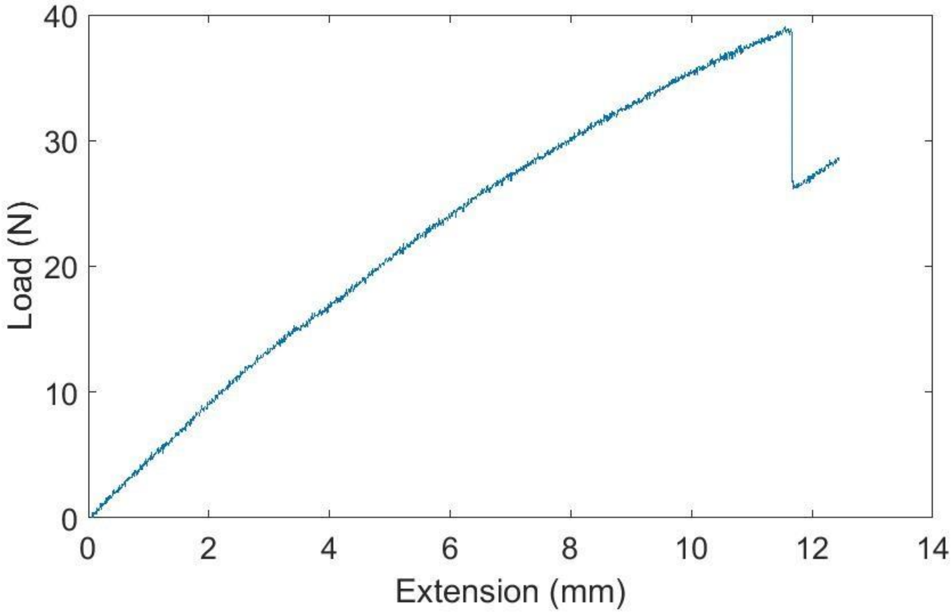

Figure B-15 Loading curve of bare ABS edge-up L-shaped sample.

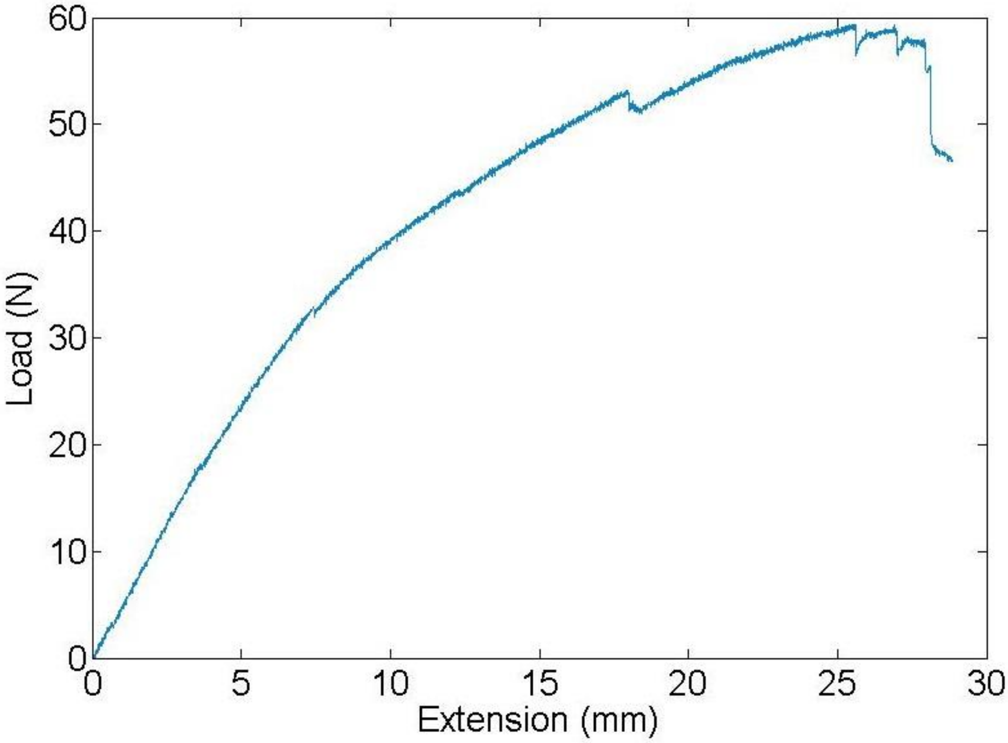

Figure B-16 Loading curve of bare ABS face-up L-shaped sample.

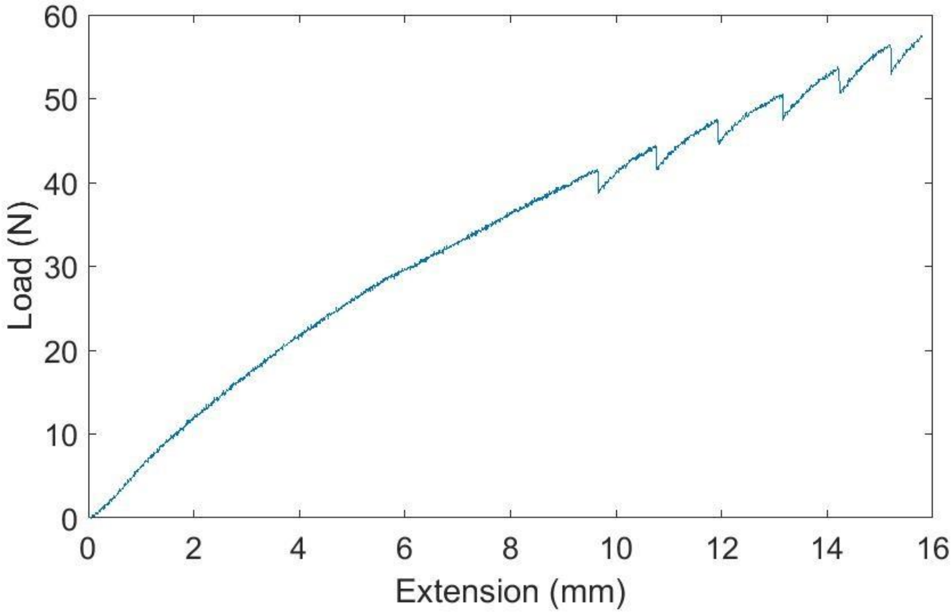

Figure B-17 Loading curve of CFRP reinforced edge-up L-shaped sample 1.

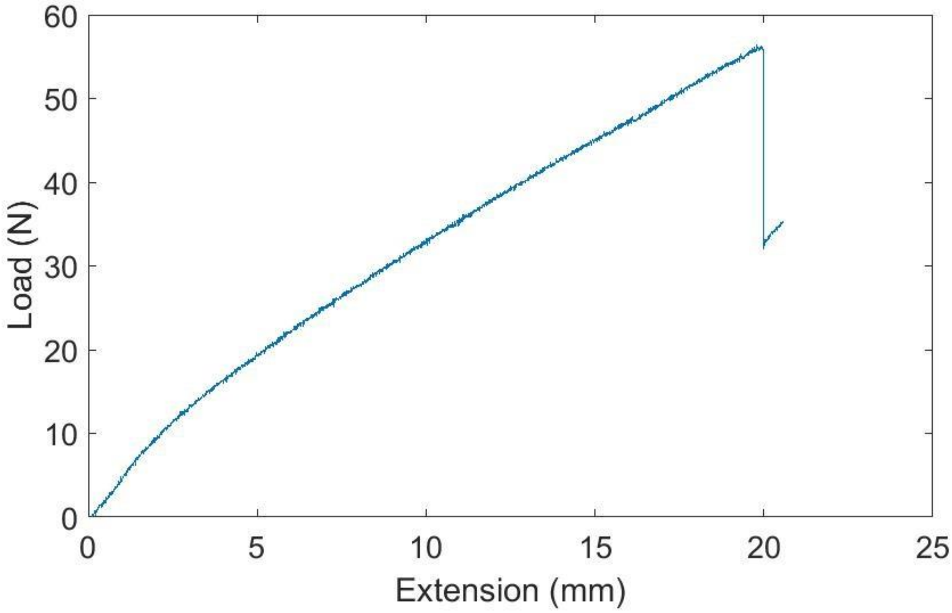

Figure B-18 Loading curve of CFRP reinforced edge-up L-shaped sample 2.

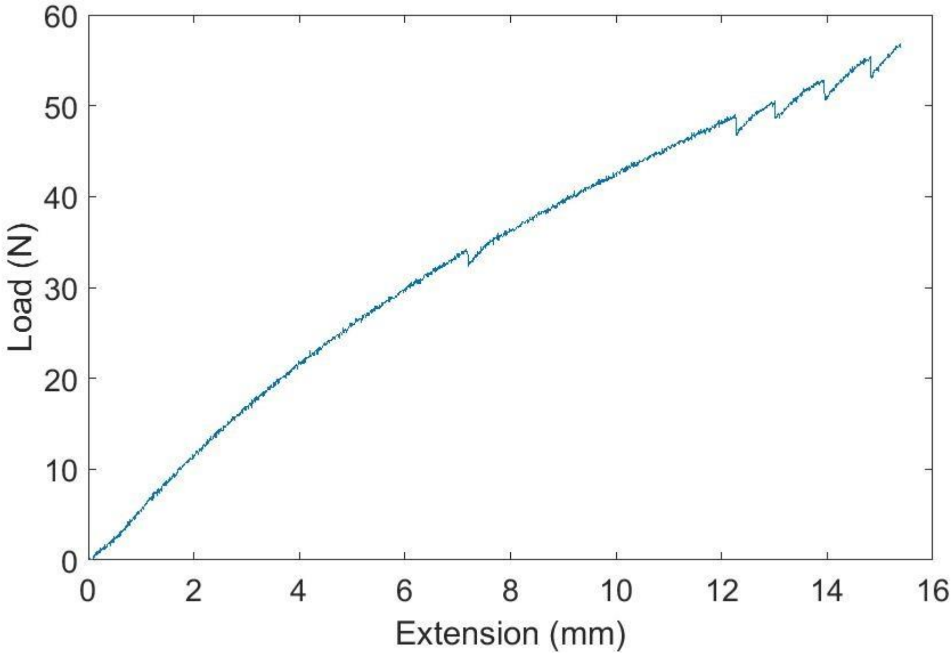

Figure B-19 Loading curve of CFRP reinforced face-up L-shaped sample 1.

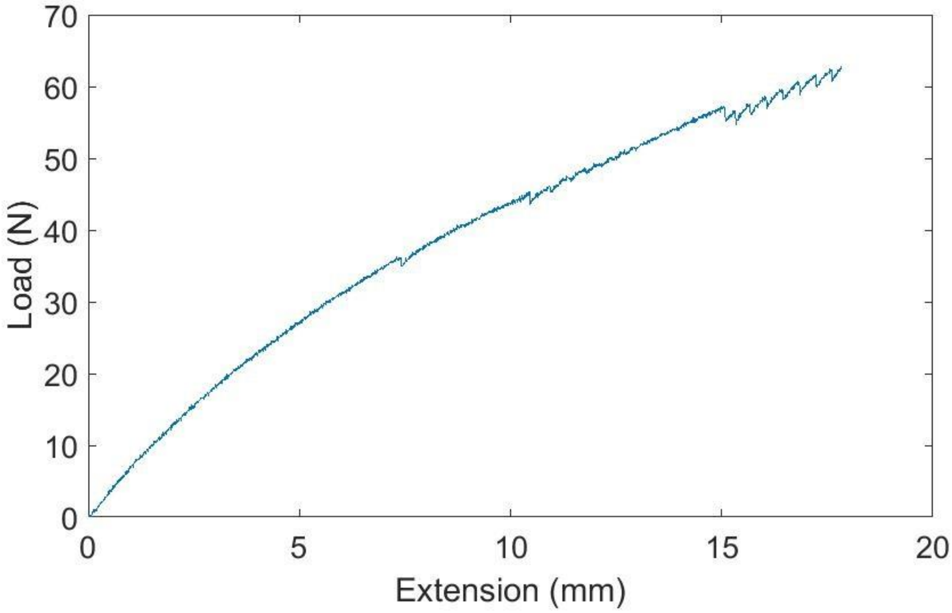

Figure B-20 Loading curve of CFRP reinforced face-up L-shaped sample 2.

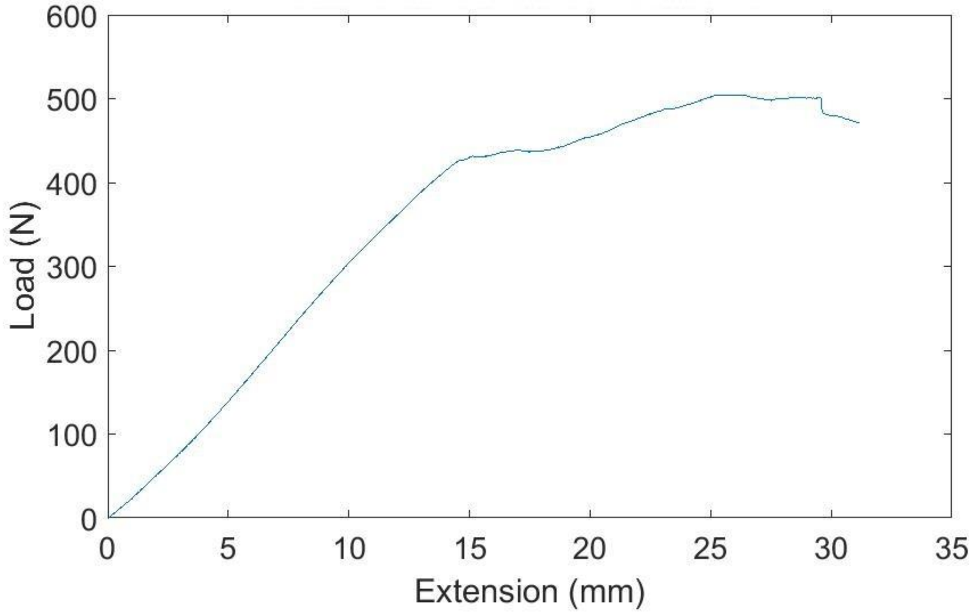

Figure B-21 Loading curve of fill compositing edge-up L-shaped sample 1.

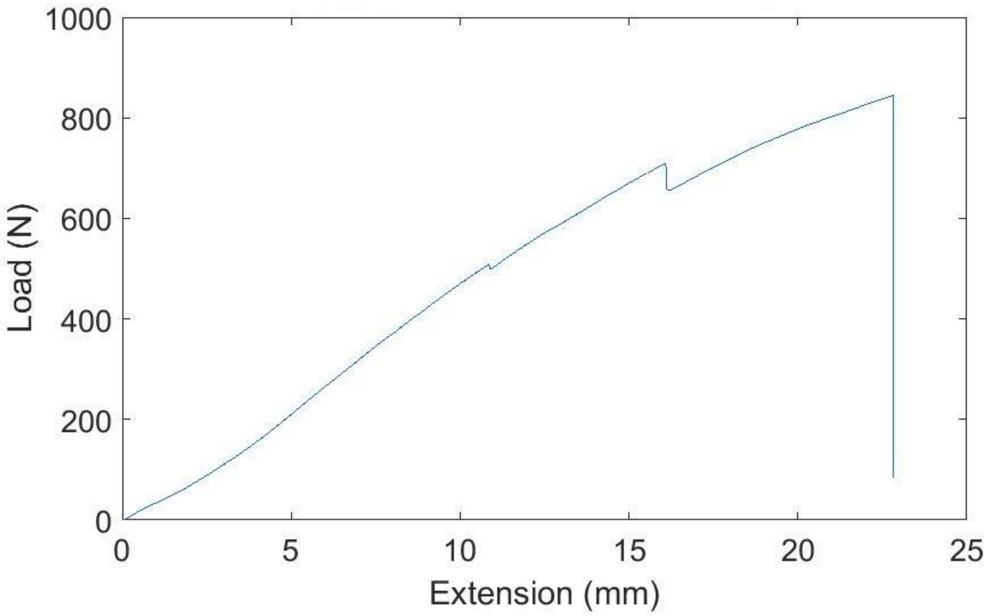

Figure B-22 Loading curve of fill compositing edge-up L-shaped sample 2.

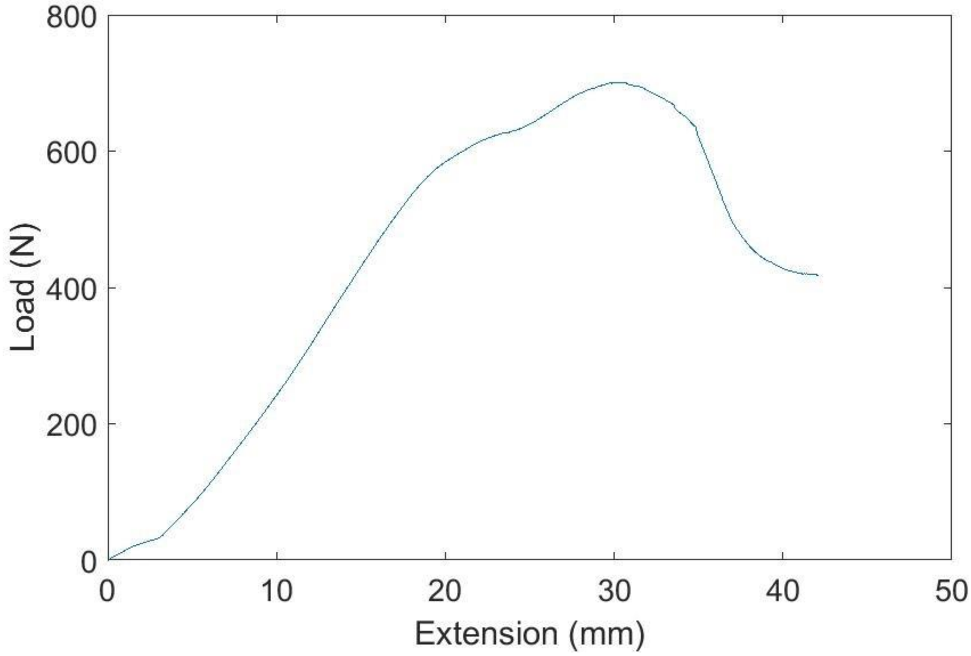

Figure B-23 Loading curve of fill compositing edge-up L-shaped sample 3.

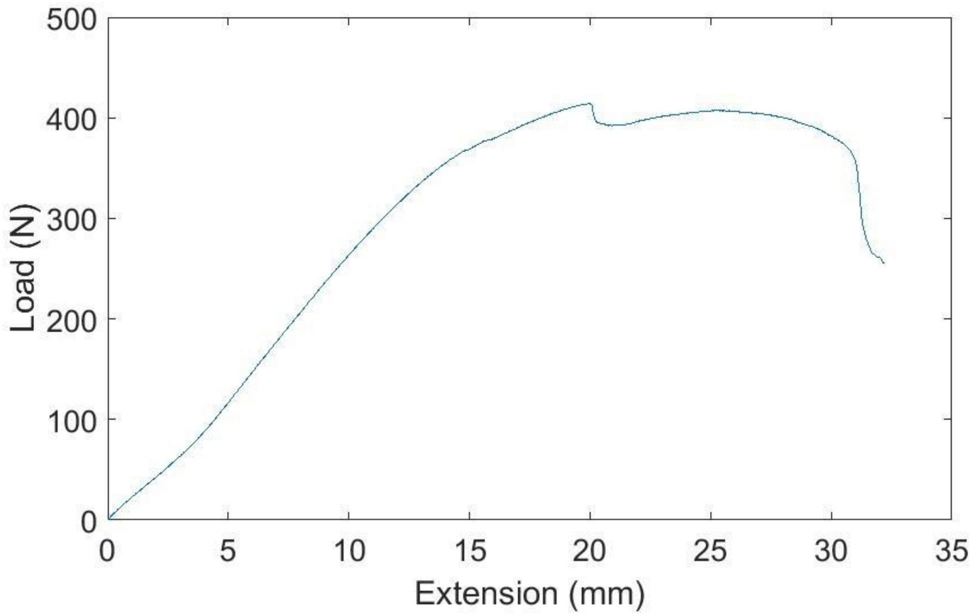

Figure B-24 Loading curve of fill compositing face-up L-shaped sample.